Electronic Structures of Active Sites in Copper Proteins: Contributions to Reactivity

EDWARD I. SOLOMON,* MICHAEL J. BALDWIN, and MICHAEL D. LOWERY

Department of Chemistry, Stanford University, Stanford, California 94305

Received December 2, 1991 (Revised Manuscript Received March 10, 1992)

Contents

I. Introduction

Spectroscopy has played a major role in developing our understanding of active sites in copper proteins. Often these sites exhibit spectral features which are unique compared to small-molecule copper complexes and which derive from the unusual geometric, and hence electronic, structures that can be imposed on the metal ion through its interaction with the protein biopolymer. It has been the goal of our research to understand the geometric and electronic structural origin of these unique spectral features and to evaluate the contribution of electronic structure to the high reactivity and selectivity of these active sites in catalysis. Studies on a number of copper proteins provide important examples of the contributions that inorganic spectroscopy has made to bioinorganic chemistry. In the initial phase of this research, a basic understanding of the origin of these unique spectral features was achieved and used to generate a spectroscopically effective working model of the metalloprotein active site. As the results of high-resolution protein crystallography become available, one can correlate the spectroscopy with the geometric structure, combine this with molecular orbital calculations and parallel spectral studies on structurally defined model complexes, and one can develop a detailed understanding of the active-site electronic structure and its contribution to biological function.

Table I presents an overview of the known copper proteins and their function and is organized by the spectral features of their active sites. The "normal" copper proteins exhibit spectral features which parallel those described for cupric chloride in the next section. Often normal copper proteins contain an additional organic cofactor which contributes intense $\pi \rightarrow \pi^*$ transitions in the visible/UV spectral region.[1] Inorganic spectroscopic studies on this class of proteins focus on defining the structures of the active sites and their interactions with small molecules, substrates, and cofactors related to the molecular mechanism. The metal ion electronic structure of normal copper proteins plays a less critical role in catalysis and thus these systems are not included in this review. At the bottom of Table I are nitrous oxide reductase and cytochrome *c* oxidase, both of which contain an unusual Cu_A center along with other copper and iron centers.[2] These have been included here for completeness; however, at this time they are not very well understood with respect to geometric and electronic structure and are not considered further in this review.

The blue copper proteins, coupled binuclear copper proteins, and multicopper oxidases all have quite unusual spectral features relative to normal cupric complexes. The blue copper proteins are involved in outer-sphere long-range electron transfer, the hemocyanins reversibly bind dioxygen, the tyrosinases activate O_2 for hydroxylation of monophenols, and the multicopper oxidases couple four one-electron oxidations of substrate to the four-electron reduction of dioxygen to water. At this time, the origins of their unique spectral features are generally clear and define important new electronic and geometric structures which play critical roles in biological function. These are the focus of the present review. Emphasis is placed on results obtained over the past 10 years as earlier work has been reviewed in ref 3. Finally, we note that the blue copper proteins are often referred to as having type 1 copper centers, the normal as having type 2, and the coupled binuclear as having type 3 centers. In this review we reserve this nomenclature for the multicopper oxidases which contain at least one of each type of copper, since we have shown[4] that the type 3 center in the oxidases is fundamentally different from that in the coupled binuclear copper proteins and that it is, in fact, part of a trinuclear copper cluster also containing the type 2 copper (see section V).

II. Normal Cupric Complexes

Since the focus of this research is on unique spectral features and electronic structures, it is important to understand the origin of parallel data on "normal" cupric complexes. The square planar (D_{4h}) $CuCl_4^{2-}$ complex serves as a most appropriate model complex. It has become one of the best understood transition metal complexes in physical–inorganic chemistry with respect

0009-2665/92/0792-0521$10.00/0

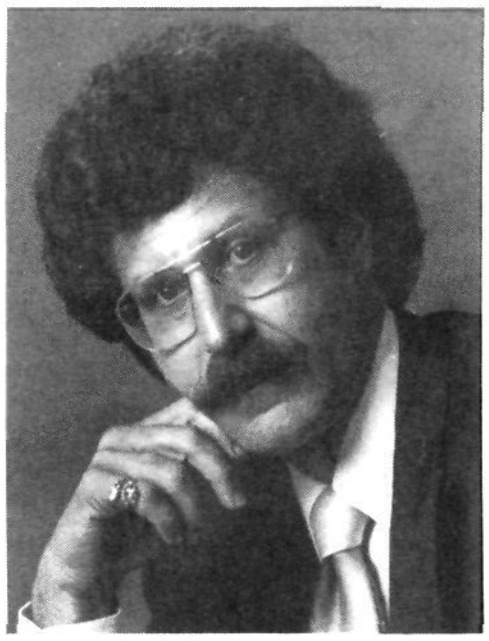

Edward I. Solomon is presently the Monroe E. Spaght Professor of Chemistry at Stanford University where he has been since 1982 and was previously a Professor at the Massachusetts Institute of Technology. Professor Solomon received his Ph.D. for research directed by Professor Donald S. McClure at Princeton University and then was a postdoctoral fellow working first with Professor C. J. Ballhausen at the H. C. Ørsted Institute at the University of Copenhagen and then with Professor Harry B. Gray at the California Institute of Technology. He is an associate editor of *Inorganic Chemistry* and a member of the editorial advisory board of *Chemical Reviews*, *Inorganic Biochemistry*, and *Chemtracts*; he has been the first Glen Seaborg, O. K. Rice, and Reilly, Frontiers and World Bank lecturer and an Invited Professor at the University of Paris, Xiamen University, China, and La Plata University, Argentina. He received the 1990 Deans Award for Distinguished Teaching at Stanford. His research interests include physical–inorganic chemistry, bioinorganic chemistry, and surface science with emphasis on the detailed spectroscopic study of transition metal ion electronic structure.

Michael J. Baldwin was born in Seattle, WA, in 1964. He received his B.S. in chemistry from Seattle University in 1986 while working in the research group of Dr. S. I. Hakomori at the Fred Hutchinson Cancer Research Center in Seattle. He is currently working toward the completion of his Ph.D. requirements at Stanford University in the research group of Professor Edward I. Solomon. His current research interests include the binding and activation of dioxygen and its redox partners by transition metals.

to its electronic structure,[5] which is now briefly reviewed. The cupric ion has nine electrons in five degenerate d orbitals in the free ion. When placed in an octahedral environment of chloride ligands, the d orbitals go up in energy and split into t_{2g} and e_g sets due to repulsive interactions with the ligands, producing a $(t_{2g})^6(e_g)^3$ configuration at lowest energy. This corresponds to a ^2E_g ground state which is orbitally degenerate and unstable to a Jahn–Teller distortion which reduces the symmetry, removes the degeneracy, and

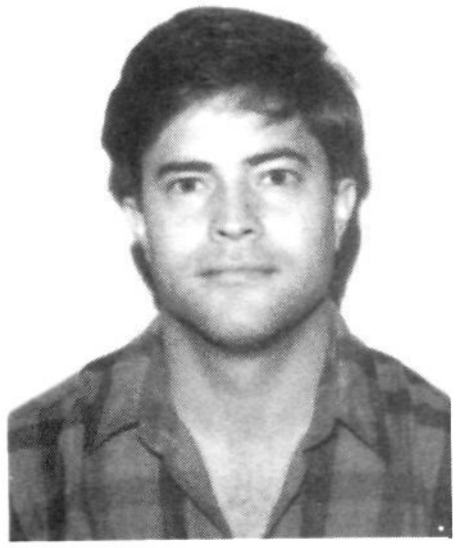

Michael D. Lowery was born in 1960 in El Paso, TX. He received his B.S. and M.S. degrees in chemistry at Illinois State University under the direction of Professor James E. House, Jr. He received his Ph.D. from the University of Illinois in 1989 under the supervision of Professor David N. Hendrickson. Currently he is following his interests in bioinorganic chemistry with a postdoctoral appointment with Professor Edward I. Solomon investigating the electronic structure of blue copper proteins.

lowers the ground state energy. The Jahn–Teller distortion normally found for cupric complexes is a tetragonal elongation (along the z axis) which results in four tightly bound ligands along the x and y axes, defining the equatorial plane (Figure 1a). A fundamental principle of ligand-field theory is that the energy splitting of the d orbitals is strongly dependent on the nature of the ligands and their geometry about the metal center. The experimental splitting found (vide infra) for D_{4h}-$CuCl_4^{2-}$ is given in Figure 1b, with the highest energy level being the $d_{x^2-y^2}$ orbital, which has the greatest repulsive interaction with the ligands as it is oriented along the equatorial Cl–Cu bonds. For the d^9 cupric ion this d orbital splitting results in one unpaired electron in the $d_{x^2-y^2}$ orbital which has b_{1g} symmetry in the D_{4h} molecular point group generating a $^2B_{1g}$ ground state, which can be studied at high resolution by EPR spectroscopy.

As shown in Figure 1c, this ground-state doublet splits linearly in a magnetic field by an amount $g\beta H$ where β is the Bohr magneton ($= 4.6686 \times 10^{-5}$ cm^{-1}/gauss), H is the external magnetic field, and the g factor is the quantity of experimental interest. An important feature of transition metal systems is that the g factor will deviate from 2.0023 and be anisotropic, that is have different values for the magnetic field oriented along ($g_\parallel$) and perpendicular to ($g_\perp$) the molecular z direction in Figure 1a. These orientations correspond to EPR turning points (i.e., extrema) which dominate the orientation-averaged spectrum associated with a frozen solution or powdered cupric complex as shown in Figure 1d. Additional features in this EPR spectrum derive from the copper nuclear spin of $^3/_2$ which interacts with the electron spin, producing a hyperfine splitting of the EPR signal into $2I + 1 = 4$ allowed ($\Delta m_I = 0$, $\Delta m_s = 1$) transitions (Figure 1c). From the spectrum in Figure 1d the hyperfine coupling constant (A) is also anisotropic with $A_\parallel$ being quite large for tetragonal cupric complexes (164×10^{-4} cm^{-1} for D_{4h}-$CuCl_4^{2-}$).[6] For D_{4h}-$CuCl_4^{2-}$, $g_\parallel$ ($= 2.221$) is greater than $g_\perp$ ($= 2.040$) which is greater than 2.0023, as required by ligand-field theory for a $d_{x^2-y^2}$ ground state. An unpaired electron in a pure $d_{x^2-y^2}$ orbital should have only spin angular

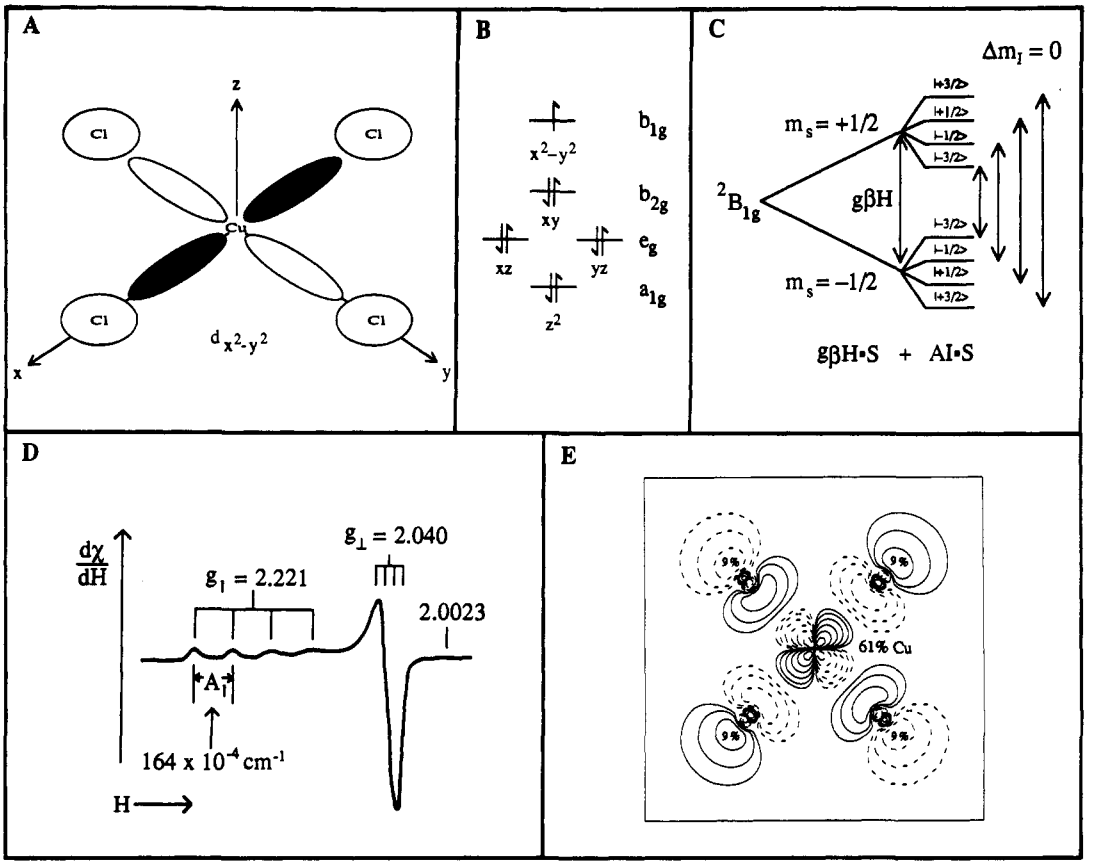

Figure 1. Ligand-field theory and ground-state electronic properties of normal cupric complexes: (A) square planar D_{4h}-$CuCl_4^{2-}$; (B) ligand field splitting of d orbitals in D_{4h} symmetry; (C) $^2B_{1g}$ ground-state Zeeman and hyperfine splitting diagram; (D) powder pattern EPR spectrum of the $^2B_{1g}$ ground state; (E) $^2B_{1g}$ ground-state wave function from adjusted-sphere SCF-Xα-SW calculation.

momentum and the g value should equal 2.0023 and be isotropic. In ligand-field theory, one allows for spin–orbit coupling of excited d orbital derived states into the ground state which results in an additional orbital angular momentum contribution to the g value. A complete ligand-field calculation of the g values for D_{4h}-$CuCl_4^{2-}$ gives[5] $g_\parallel$ (= 2.743) which is greater than $g_\perp$ (= 2.177), in general agreement with experiment but quantitatively larger than observed. This indicates that there is too much orbital angular momentum in the ground state in this ligand-field calculation and requires that one allow for covalent delocalization of the metal d orbitals onto the ligand valence orbitals.

A quantum mechanical method that has proved to be particularly powerful in describing the electronic structure and bonding in transition metal complexes is the self-consistent field-Xα-scattered wave (SCF-Xα-SW) approach developed by Slater and Johnson.[7] This method has been applied[8-10] to generate an electronic structure description of D_{4h}-$CuCl_4^{2-}$ and the resulting wave functions have been used to calculate the ground state g values. The values obtained ($g_\parallel$ = 2.144, $g_\perp$ = 2.034) are indeed reduced from the ligand field calculated values. However, they are smaller than the experimental values, indicating that this calculation is providing a description of the bonding which is too covalent. In this type of calculation there is a set of parameters, the sphere sizes used in setting up the scattered wave solution, which is somewhat arbitrarily fixed at what is known as their Norman radii.[11] These sphere radii can, in fact, be systematically varied.[9,10,12] Increasing the sphere size on the metal while matching the potential at the boundary with the ligand sphere shifts electron density onto the metal, lowers its effective nuclear charge, and reduces its covalent interaction with the ligand valence orbitals. Varying the sphere radii until the ground state g values obtained from the Xα calculation agree with the experimental values provides an experimentally adjusted description of the electronic structure of the transition metal complex. This procedure gives[13] the ground-state wave function for D_{4h}-$CuCl_4^{2-}$ shown in Figure 1e which has 61% Cu(II) $d_{x^2-y^2}$ character with the rest of the wave function being delocalized equivalently into the $3p_\sigma$ orbitals of the four chloride ligands as required by symmetry. There are a variety of spectroscopic methods allowing this description of the covalency to be tested experimentally. One particularly powerful method is variable-energy photoelectron spectroscopy using synchrotron radiation which is described in ref 14. For D_{4h}-$CuCl_4^{2-}$ all methods give a value within 5% of that obtained from the SCF-Xα-SW calculation adjusted to the ground-state spin-Hamiltonian parameters supporting a high level of confidence in the ground-state bonding description.

With respect to the excited states of D_{4h}-$CuCl_4^{2-}$, photons with energies in the 12 500–17 000-cm^{-1} (575–800-nm) region, will excite electrons from the filled d levels into the $^1/_2$ occupied $d_{x^2-y^2}(b_{1g})$ level as illustrated in Figure 2a. These are d→d or ligand-field transitions which are Laporté (i.e. parity) forbidden and hence are weak in the absorption spectrum with ϵ's (molar extinction coefficients) of less than 50 M^{-1} cm^{-1} (Figure 2b). There are three possible d→d transitions for

TABLE I. Copper Proteins[§]

Normal Copper Enzymes

normal copper enzymes	molecular weight (in kDa), subunits, no. of Cu	function	cofactor[‖]	ref
copper–zinc superoxide dismutase*	31, α_2, 2	$2O_2^- + 2H^+ \rightarrow H_2O_2 + O_2$		*a*
diamine oxidases	160–200, α_2, 2	$R'CHNR_2 + O_2 + H_2O \rightarrow R'CHO + HNR_2$	6-hydroxydopa (TOPA)	*b*
dopamine β monooxygenase	290, α_4, 4 or 8	dopamine + ascorbate + O_2 → noradrenaline + dehydroascorbate + H_2O		*c*
galactose oxidase*	32, –, 1	$RCH_2OH + O_2 \rightarrow RCHO + H_2O_2$	tyrosine radical	*d*
phenylalanine hydroxylase	68, –, 1	phenylalanine + O_2 → tyrosine + H_2O	tetrahydropterin	*e*
neurocuprein	9, –, 1	adrenaline/adrenochrome equilibrium?		*f*

Blue Copper Proteins

blue copper proteins[#] [function: electron transfer]	molecule weight, Da	redox potential, mV (pH)	blue band energy, nm (ϵ, M^{-1} cm^{-1})	EPR: $A \times 10^{-4}$ cm^{-1} $g_\parallel$ / g_z	$g_\perp$ g_y	$g_\perp$ g_x	$A_\parallel$ / A_z	$A_\perp$ A_y	$A_\perp$ A_x	ref
plastocyanin*,[‡]	10500	+370 (7.0)	597 (4500)	2.226	2.059	2.042	63			*h*
azurins										*i*
*Alcaligenes denitrificans**	14000	+276 (7.0)	619 (5100)	2.255	2.059		60			22
Alcaligenes faecalis S-6*	14000	+266 (7.0)	593							21b
*Pseudomonas aeruginosa**	14600	+308 (7.0)	631 (3800)	2.260	2.052		60			
*Pseudomonas denitrificans**	14600			2.260	2.055		60			
stellacyanin	20000	+184 (7.1)	609 (3400)	2.287	2.077	2.025	37	28	54	*j*
amicyanin[†]	13800	+261 (7.0)	596 (3950)	2.239	2.046		59	36		*k*
auracyanin	12800	+240 (8.0)	596 (2900)	2.210	2.062	2.018	47	12	62	*l*
cucumber basic blue*	10100	+317 (7.0)	597 (4500)	2.207	2.08	2.02	55	10	60	*m*
mavicyanin	18000	+285 (7.0)	600 (5000)	2.287	2.077	2.025	37	28	54	*n*
rusticyanin	16500	+680 (2.0)	597 (2240)	2.229	2.064	2.019	47	19	61	*o*
umecyanin	14600	+283 (7.0)	610 (3400)	2.317	2.05		38			*p*

Normal + Blue Copper Enzymes

normal + blue copper enzymes[◇] [function: $NO_2^- \rightarrow NO$]	molecular weight (in kDa), subunits, no. of Cu	blue band energy, nm (ϵ, M^{-1} cm^{-1})	EPR parameters $g_\parallel$	EPR parameters $A_\parallel$ ($\times 10^{-4}$ cm^{-1})	ref
nitrite reductase					
*Achromobacter cycloclastes**	69, α_2, 6	590 (2000)	type 1 2.195 type 2 2.262	type 1 73 type 2 175	*q*

Binuclear Copper Proteins

binuclear copper proteins[‡]	molecular weight, kDa, per Cu_2 site[▽]	$O_2^{2-} \rightarrow Cu$ CT bands,[§] nm (ϵ, M^{-1} cm^{-1})	function	ref
molluscan hemocyanins			O_2 transport	*t*, *u*
Busycon canaliculatum	50	350 (~20000) 570 (1000) 480 (CD band)	(catalase activity: $2H_2O_2 \rightarrow 2H_2O + O_2$)	
arthropodan hemocyanins			O_2 transport	39, 56, *t*, *u*
*Panulirus interruptus**	75	335 (~20000) 580 (800) 510 (CD band)	(no catalase activity)	
*Limulus polyphemus**	75	340 (~20000) 590 (1000) 500 (CD band)	(no catalase activity)	
tyrosinase				62, 63, *v*
Neurospora crassa	42	345 (~20000) 590 (~1000) 520 (CD band)	$O_2 + 2H^+ +$ monophenol → *o*-diphenol + H_2O $O_2 + 2$ o-diphenol → 2 o-quinone + $2H_2O$ (catalase activity)	

Multicopper Oxidases

multicopper oxidases[68] [function: $O_2 + 4H^+ + 4e^- \rightarrow 2H_2O$ coupled to 4 one-electron oxidations of substrate]	molecular weight, kDa	no. and type of copper center	EPR parameters $g_\parallel$	EPR parameters $g_\perp$	$A_\parallel \times 10^{-4}$, cm^{-1}	absorption band, nm (ϵ, M^{-1} cm^{-1})
laccase						
Fungal: *Polyspora versicolor*	60–90	1 type 1	2.19	2.03	90	610 (4900)
(*p*-diphenol: O_2 oxidoreductase)		1 type 2	2.24	2.04	194	
		1 type 3				330 (2700)
Tree: *Rhus vernicifera*	110–140	1 type 1	2.23	2.05	43	615 (5700)
(monophenol, dihydroxyphenylalanine: O_2 oxidoreductase)		1 type 2	2.24	2.05	200	
		1 type 3				330 (2800)
ascorbate oxidase*,[34]	145	2 type 1	2.227	2.058, 2.036	58	610 (4800)
(L-ascorbate: O_2 oxidoreductase)		2 type 2	2.242	2.053	199	
		2 type 3				330 (2000)
ceruloplasmin or ferroxidase I	130	1st type 1	2.215	2.06	92	610 (10000)
(iron(II): O_2 oxidoreductase)		2nd type 1	2.206	2.05	72	610 (10000)
		1 type 2	2.247	2.06	189	
		1 type 3				330 (3300)

Cu_A-Containing Enzymes

Cu_A-containing enzymes	molecular weight (in kDa), subunits	metal centers	function	ref
cytochrome c oxidase	170, 12	hemes (Fe_a and Fe_{a3}), Cu_A, Cu_B	$O_2 + 4$ ferrocytochrome c + $4H^+ \rightarrow$	2b, *w*

TABLE I (Continued)

Cu_A-Containing Enzymes				
Cu_A-containing enzymes	molecular weight (in kDa), subunits	metal centers	function	ref
		(Cu_B antiferromagnetically coupled to Fe_{a3})	$2H_2O$ + 4 ferricytochrome c	
nitrous oxidase reductase			$N_2O + 2e^- + 2H^+ \rightarrow N_2 + H_2O$	*x*
Pseudomonas stutzeri	140, α_2	2 Cu_A, 6 other Cu atoms		
Pseudomonas aeruginose	73, α_2	4 Cu atoms/molecule		

[g] In addition to the proteins listed in Table I other proteins which have been suggested to require copper for activity are listed in footnote *y*. [*] A high-resolution x-ray crystal structure has been reported. [†] Preliminary crystallographic data have been reported. See references for details. [‡] A NMR structure has been reported. [a] (1) Valentine, J. S.; Pantoliano, M. W. In *Copper Proteins*; Spiro, T. G., Ed.; Wiley-Interscience: New York, 1981; pp 291–358. (2) Strothkamp, K. G.; Lippard, S. J. *Acc. Chem. Res.* **1982**, *15*, 318–326. (3) Fee, J. A.; Peisach, J.; Mims, W. B. *J. Biol. Chem.* **1981**, *256*, 1910–1914. (4) Fielden, E. M.; Rotilio, G. In *Copper Proteins and Copper Enzymes*; Lontie, R., Ed.; CRC Press: Boca Raton, FL, 1984; Vol. II, Chapter 2. (5) For a 2.0-Å X-ray crystal structure of bovine erythrocyte Cu,Zn SOD, see: Tainer, J. A.; Getzoff, E. D.; Beem, K. M.; Richardson, J. S.; Richardson, D. C. *J. Mol. Biol.* **1982**, *160*, 181–217. Tainer, J. A.; Getzoff, E. D.; Richardson, J. S.; Richardson, D. C. *Nature* **1983**, *306*, 284–287. (6) For a 2.5-Å resolution structure of yeast SOD, see: Djinovic, K.; Gatti, G.; Coda, A.; Antolini, L.; Pelosi, G.; Desideri, A.; Falconi, M.; Marmocchi, F.; Rotilio, G.; Bolognesi, M. *Acta Crystallogr.* **1991**, *B47*, 918–927. [b] (1) Dooley, D. M. *Life Chem. Rep.* **1987**, *5*, 91–154. (2) *Structure and Functions of Amine Oxidases*; Mondovi, B., Ed.; CRC Press: Boca Raton, FL, 1985. (3) Knowles, P. F.; Yadav, K. D. S. In *Copper Proteins and Copper Enzymes*; Lontie, E., Ed.; CRC Press: Boca Raton, FL, 1984; Vol. II, Chapter 4. [c] (1) Ljones, T.; Skotland, T. In *Copper Proteins and Copper Enzymes*; Lontie, R., Ed.; CRC Press: Boca Raton, FL, 1984; Vol. II, Chapter 5. (2) Villafranca, J. J. In *Copper Proteins*; Spiro, T. G., Ed.; Wiley-Interscience: New York, 1981; Chapter 7. [d] (1) Ettinger, M. J.; Kosman, D. J. In *Copper Proteins*; Spiro, T. G., Ed.; Wiley-Interscience: New York, 1981; Chapter 6. (2) See reference 1c for X-ray structure. [e] Benkovic, S.; Wallick, D.; Bloom, L.; Gaffney, B. J.; Domanico, P.; Dix, T.; Pember, S. *Biochem. Soc. Trans.* **1985**, *13*, 436–438. See reference 1a for cofactor. [f] (1) Mikaelyan, M. V.; Nalbandyan, R. M. *Neurochem. Int.* **1988**, *13*, 435–438. (2) Mikaelyan, M. V.; Nalbandyan, R. M. *Neurochem. Int.* **1985**, *7*, 1073–1078. (3) Sharoyan, S. G.; Shaljian, A. A.; Nalbandyan, R. M.; Buniatian, H. C. H. *Biochim. Biophys. Acta* **1977**, *493*, 478–487. [g] For recent reviews see: (1) Adman, E. T. In *Advances in Protein Chemistry*; Anfinsen, C. B., Edsall, J. T., Richards, F. M.; Eisenberg, D. S., Eds.; Academic Press: San Diego, 1991; Vol. 42, pp 145–198. (2) Sykes, A. G. *Struct. Bond.* **1991**, *75*, 175–224. (3) Sykes, A. G. *Adv. Inorg. Chem.* **1991**, *36*, 377–408. (4) Farver, O.; Pecht, I. *Coord. Chem. Rev.* **1989**, *94*, 17–45. (5) Gray, H. B. *Chem. Soc. Rev.* **1986**, *15*, 17–30. (6) Lappin, A. G. In *Metal Ions in Biological Systems*; Sigel, H., Ed.; Dekker: New York, 1981; Vol. 13; Chapter 2. (7) Adman, E. T. *Top. Mol. Struct. Biol.* **1985**, *6*, 1–42. [h] Data shown here are for spinach plastocyanin (see *g*). For the NMR-determined structure of french bean plastocyanin see: Moore, J. M.; Lepre, C. A.; Gippert, G. P.; Chazin, W. J.; Case, D. A.; Wright, P. E. *J. Mol. Biol.* **1991**, *221*, 533–555. X-ray structures exist for poplar plastocyanin: see ref 20 and Guss, J. M.; Freeman, H. C. *J. Mol. Biol.* **1983**, *169*, 521–563. For Cu(I) poplar plastocyanin, see: Guss, J. M.; Harrowell, P. R.; Murata, M.; Norris, V. A.; Freeman, H. C. *J. Mol. Biol.* **1986**, *192*, 361–387. [i] For the X-ray structure for *A. denitrificans*, see: ref 22. For *A. faecalis* S-6, see: ref 21b. For *P. aeruginosa*, see: Nar, H.; Messerschmidt, A.; Huber, R.; van de Kamp, M.; Canters, G. W. *J. Mol. Biol.* **1991**, *221*, 765–772. For *P. denitrificans*, see: ref 22. [j] Peisach, J.; Levine, W. G.; Blumberg, W. E. *J. Biol. Chem.* **1967**, *242*, 2847–2858. [k] The data shown are for *Thiobacillus versutus*, see: (1) Houwelingen, T. V.; Canters, G. W.; Stobbelaar, G.; Duine, J. A.; Frank, J.; Tsugita, A. *Eur. J. Biochem.* **1985**, *153*, 75–80. (2) Lommen, A.; Canters, G. W.; van Beeumen, J. *Eur. J. Biochem.* **1988**, *176*, 213–223. (3) Lommen, A.; Canters, G. W. *J. Biol. Chem.* **1990**, *265*, 2768–2774. (4) A preliminary X-ray structure has been reported: Petratos, K.; Dauter, Z.; Wilson, K. S.; Lommen, A.; van Beeumen, J.; Canters, G. W. *J. Mol. Biol.* **1988**, *199*, 545–546. Additional amicyanin include organism 4025: Lawton, S. A.; Anthony, C. *Biochem. J.* **1985**, *228*, 719–726. *Paracoccus denitrificans*: (1) Husain, M.; Davidson, V. L. *J. Biol. Chem.* **1985**, *260*, 14626–14629. (2) Husian, M.; Davidson, V. L.; Smith, A. J. *Biochemistry* **1986**, *25*, 2431–2436. (3) Sharma, K. D.; Loehr, T.; Sanders-Loehr, J.; Husain, M.; Davidson, V. L. *J. Biol. Chem.* **1988**, *263*, 3303–3306. *Pseudomonas* AM1: (1) Tobari, J.; Harada, Y. *Biochem. Biophys. Res. Commun.* **1981**, *101*, 502–508. (2) Ambler, R. P.; Tobari, J. *Biochem. J.* **1985**, *232*, 451–457. *Methylomonas* J: Ambler, R. P.; Tobari, J. *Biochem. J.* **1989**, *261*, 495–499. [l] Trost, J. T.; McManus, J. D.; Freeman, J. C.; Ramakrishna, B. L.; Blankenship, R. E. *Biochemistry* **1988**, *27*, 7858–7863. [m] (1) Colman, P. M.; Freeman, H. C.; Guss, J. M.; Murata, M.; Norris, V. A.; Ramshaw, J. A. M.; Venkatappa, M. P.; Vickery, L. E. *J. Mol. Biol.* **1977**, *112*, 649–650. (2) Murata, M.; Begg, G. S.; Lambrou, F.; Leslie, B.; Simpson, R. J.; Freeman, H. C.; Morgan, F. J. *Proc. Natl. Acad. Sci. U.S.A.* **1982**, *79*, 6434–6437. (3) A 3.0-Å resolution X-ray structure has been reported, see: Guss, J. M.; Merritt, E. A.; Phizackerley, R. P.; Hedman, B.; Murata, M.; Hodgson, K. O.; Freeman, H. C. *Science* **1988**, *241*, 806–811. [n] Marchesini, A.; Minelli, M.; Merkle, H.; Kroneck, P. M. H. *Eur. J. Biochem.* **1979**, *101*, 77–84. [o] (1) Cobley, J. G.; Haddock, B. A. *FEBS Lett.* **1975**, *60*, 29–33. (2) Cox, J. D.; Boxer, D. H. *Biochem. J.* **1978**, *174*, 497–502. (3) Ingledew, W. J.; Cobley, J. C. *Biochim. Biophys. Acta* **1980**, *590*, 141–158. (4) Ingledew, W. J. *Biochim. Biophys. Acta* **1982**, *683*, 89–117. (5) Cox, J. C.; Aasa, R.; Malmström, B. G. *FEBS Lett.* **1978**, *93*, 157–160. [p] Paul, K. G.; Stigbrand, T. *Biochim. Biophys. Acta* **1970**, *221*, 255–263. [q] Data shown are for *Achromobacter cycloclastes*. For a 2.3-Å X-ray crystal structure, see: (1) Godden, J. W.; Turley, S.; Teller, D. C.; Adman, E. T.; Liu, M. Y.; Payne, W. J.; LeGall, J. *Science* **1991**, *253*, 438–442. (2) Fenderson, F. F.; Kumar, S.; Adman, E. T.; Liu, M. Y.; Payne, W. J.; LeGall, J. *Biochemistry* **1991**, *30*, 7180–7185. (3) Suzuki, S.; Yoshimura, T.; Kohzuma, T.; Shidara, S.; Masuko, M.; Sakurai, T.; Iwasaki, H. *Biochem. Biophys. Res. Commun.* **1989**, *164*, 1366–1372. (4) Hulse, C. L.; Averill, B. A.; Tiedje, J. M. *J. Am. Chem. Soc.* **1989**, *111*, 2322–2323. (5) Dooley, D. M.; Moog, R. S.; Liu, M. Y.; Payne, W. J.; LeGall, J. *J. Biol. Chem.* **1988**, *263*, 14625–14628. (6) Kashem, M. A.; Dunford, H. B.; Liu, M. Y.; Payne, W. J.; LeGall, J. *Biochem. Biophys. Res. Commun.* **1987**, *145*, 563–568. (7) Liu, M. Y.; Liu, M. C.; Payne, W. J.; LeGall, J. *J. Bacteriol.* **1986**, *166*, 604–608. (8) Iwasaki, H.; Noji, S.; Shidara, S. *J. Biochem. (Tokyo)* **1975**, *78*, 355–361. *Pseudomonas aureofaciens*: Zumft, W. G.; Gotzmann, D. J.; Kroneck, P. M. H. *Eur. J. Biochem.* **1987**, *168*, 301–307. *Pseudomonas aeruginosa*: Karapetian, A. V.; Kamalian, M. G.; Malbandyan, R. M. *FEBS Lett.* **1986**, *203*, 131–134. *Nitrosomonas europaea*: (1) Miller, D. J.; Nicholas, D. J. D. *J. Gen. Microbiol.* **1985**, *131*, 2851–2854. (2) Miller, D. J.; Wood, P. M. *J. Gen. Microbiol.* **1983**, *129*, 1645–50. From *Alcaligenes* sp. NCIB 11015: (1) Sakurai, T.; Suzuki, S.; Nakahara, A.; Masuko, M.; Iwasaki, H. *Chem. Lett.* **1985**, *9*, 1297–1300. (2) Masuko, M.; Iwasaki, H.; Sakurai, T.; Suzuki, S.; Nakahara, A. *J. Biochem. (Tokyo)* **1984**, *96*, 447–454. *Rhodopseudomonas sphaeroides* forma sp. *denitrificans*: Michalski, W. P.; Nicholas, D. J. D. *Biochim. Biophys. Acta* **1985**, *828*, 130–7. From *Alcaligenes* sp: Sano, M.; Matsubara, T. *Chem. Lett.* **1984**, *12*, 2121–2124. *Alcaligenes faecalis* S6: (1) Kakutani, T.; Watanabe, H.; Arima, K.; Beppu, T. *J. Biochem. (Tokyo)* **1981**, *89*, 463–472. (2) Kakutani, T.; Watanabe, H.; Arima, K.; Beppu, T. *J. Biochem. (Tokyo)* **1981**, *89*, 453–461. A preliminary X-ray structure has been reported: Petratos, K.; Beppu, T.; Banner, D. W.; Tsernoglou, D. *J. Mol. Biol.* **1986**, *190*, 135. [r] Molecular weights are given per binuclear site. For molluscan hemocyanins, there are approximately 20 subunits per molecule, each containing 8 oxygen-binding domains of the given molecular weight. Arthropodan hemocyanins have dissociable subunits of the given molecular weight, each containing a single oxygen-binding site, with as many as 48 subunits per molecule assembled as hexamers, depending on the species. Tyrosinase has a single active site per molecule. [s] These spectral features are for the oxy form of the protein, which is the resting form for the hemocyanins. The resting form of tyrosinase is the met form. [t] Nickerson, K. W.; van Holde, K. E. *Comp. Biochem. Physiol.* **1971**, *39B*, 855–872. [u] Himmelwright, R. S.; Eickman, N. C.; LuBien, C. D.; Solomon, E. I. *J. Am. Chem. Soc.* **1980**, *102*, 5378–5388. [v] Lerch, K. *FEBS Lett.* **1976**, *69*, 157–160. [w] (1) Kroneck, P. M.; Antholine, W. E.; Kastrau, D. H. W.; Buse, G.; Steffens, G. C. M.; Zumft, W. G. *FEBS Lett.* **1990**, *268*, 274–276. (2) Larsen, R. W.; Ondrias, M. R.; Copeland, R. A.; Li, P. M.; Chan, S. I. *Biochemistry* **1989**, *28*, 6418–6422. [x] References for *Pseudomonas stutzeri*: (1) Dooley, D. M.; McGuirl, M. A.; Rosenzweig, A. C.; Landin, J. A.; Scott, R. A.; Zumft, W. G.; Devlin, F.; Stephens, P. J. *Inorg. Chem.* **1991**, *30*, 3006–3011. (2) Zumft, W. G.; Viebrock-Sambale, A.; Braun, C. *Eur. J. Biochem.* **1990**, *192*, 591–599. (3) Riester, J.; Zumft, W. G.; Kroneck, P. M. H. *Eur. J. Biochem.* **1989**, *178*, 751–762. (4) Dooley, D. M.; Moog, R. S.; Zumft, W. G. *J. Am. Chem. Soc.* **1987**, *109*, 6730–6735. (5) Scott, R. A.; Zumft, W. G.; Coyle, C. L.; Dooley, D. M. *Proc. Natl. Acad. Sci. U.S.A.* **1989**, *86*, 4082–4086. (6) Kroneck, P. M. H.; Antholine, W. A.; Riester, J.; Zumft, W. G. *FEBS Lett.* **1988**, *242*, 70–74. (7) Coyle, C. L.; Zumft, W. G.; Kroneck, P. M. H. *Life Chem. Rep.* **1987**, *5*, 289–303. (8) Dooley, D. M.; Moog, R. S.; Zumft, W. G. *J. Am. Chem. Soc.* **1987**, *109*, 6730–6735. (9) Zumft, W. G.; Matsubara, T. *FEBS Lett.* **1982**, *148*, 107–112. (10) Coyle, C. L.; Zumft, W. G.; Kroneck, P. M. H.; Körner, H.; Jakob, W. *Eur. J. Biochem.* **1985**, *153*, 459–467. *Alcaligenes* sp: Matsubara, T.; Sano, M. *Chem. Lett.* **1985**, *7*, 1053–1056. *Paracoccus denitrificans*: Snyder, S. W.; Hollocher, T. C. *J. Biol. Chem.* **1987**, *262*, 6515–6525. *Pseudomonas aeruginosa*: (1) SooHoo, C. K.; Hollocher, T. C.; Kolodziej, A. F.; Orme-Johnson, W. H.; Bunker, G. *J. Biol. Chem.* **1991**, *266*, 2210–2218. (2) SooHoo, C. K.; Hollocher, T. C. *J. Biol. Chem.* **1991**, *266*, 2203–2209. *Achromobacter cycloclastes*: (1) Hulse, C. L.; Averill, B. A. *Biochem. Biophys. Res. Commun.* **1990**, *166*, 729–735. [y] (1) Bilirubin oxidase: Gotoh, Y.; Kondo, Y.; Kaji, J.; Takeda, A.; Samejima, T. *J. Biochem.* **1989**, *106*, 621–626. (2) Glycerol oxidase: Uwajima, T.; Shimizu, Y.; Terada, O. *J. Biol. Chem.* **1984**, *259*, 2748–2753. (3) Methane monooxygenase: (a) Shiemke, A. K.; DiSpirito, A. A.; Lidstrom, M. E.; Chan, S. I. *J. Inorg. Biochem.* **1991**, *43*, 191. (b) Tonge, G. M.; Harrison, D. E. F.; Higgins, I. J. *Biochem. J.* **1977**, *161*, 333–344. (4) Peptidyl-glycine α-amidating monooxygenase (PAM): Eipper, B. A.; Mains, R. E.; Glembotski, C. C. *Proc. Natl. Acad. Sci. U.S.A.* **1983**, *80*, 5144–5148. (5) Ferroxidase II: Garnier, A.; Tosi, L.; Steinbuch, M. *Biochem. Biophys. Res. Commun.* **1981**, *98*, 66–71. (6) Uridine nucleosidase: Magni, G.; Natalini, P.; Ruggieri, S.; Vita, A. *Biochem. Biophys. Res. Commun.* **1976**, *69*, 724–730. (7) Quercetinase: Oka, T.; Simpson, F. J. *Biochem. Biophys. Res. Commun.* **1971**, *43*, 1–5. (8) Phenylethylamine oxidase: Shimizu, E.; Ichise, H.; Yorifuji, T. *Agric. Biol. Chem.* **1990**, *54*, 851–853.

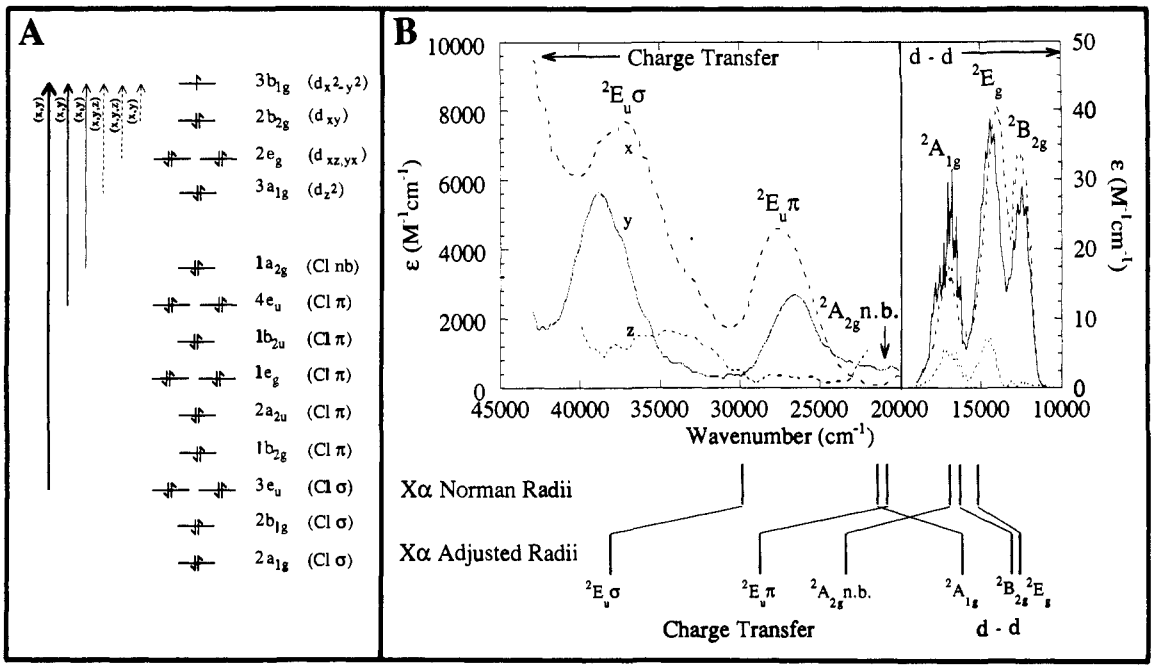

Figure 2. Ligand-to-metal charge transfer (LMCT) and ligand field spectra for D_{4h}-$CuCl_4^{2-}$: Part A shows a molecular orbital energy level diagram. Experimentally observed transitions are depicted by the vertical arrows, d→d transitions are dashed, and LMCT are solid lines. The boldness of the arrows indicates the relative intensity of the transition, and the polarizations for each transition is listed in parentheses. Part B shows polarized single-crystal spectra for D_{4h}-$CuCl_4^{2-}$. The excited-state transition assignment is listed above each band maximum. The fine structure in the ligand-field transition derives from vibronic coupling. Below the figure (to the same energy scale) are the SCF-Xα-SW predicted transition-state energies using the Norman radii and the adjusted sphere radii as described in the text.

copper(II) in D_{4h} symmetry which are made allowed through coupling with odd parity vibrations. A combination of group theory derived selection rules and polarized single-crystal absorption spectra lead to the assignments[15] of these ligand-field transitions given at the top of the bands in Figure 2b, which in turn generate the energy order of the d orbitals given in Figure 2a (and Figure 1b). At higher energy (>25 000 cm^{-1}, <400 nm), as in Figure 2b, are the Laporté-allowed intense ($\epsilon \sim$ 5000–10 000 M^{-1} cm^{-1}) ligand-to-metal charge transfer transitions,[8] which correspond to optical excitation of an electron from a filled chloride-centered level to the half-occupied copper-centered $d_{x^2-y^2}$ orbital in Figure 2a. Note that each chloride has three valence 3p orbitals which split in energy due to bonding interactions with the metal ion; those involved in σ bonding are at deepest binding energy due to their greater ligand–metal overlap. The overlap of the donor and acceptor orbitals involved in the charge-transfer process also governs the intensity of a charge-transfer transition, and since the half-occupied $d_{x^2-y^2}$ level has only σ overlap with the ligands, the charge-transfer transition of greatest intensity should be the Cl p_σ-e_u → Cu $d_{x^2-y^2}$($^2B_{1g}$ → $^2E_u(\sigma)$) transition which is electric dipole allowed and x,y polarized. The allowed $^2B_{1g}$ → $^2E_u(\pi)$ charge-transfer transition involves excitation of an electron from a π-bonding ligand valence orbital into the Cu $d_{x^2-y^2}$ level and thus should have no intensity. However, it configurationally interacts with the $^2E_u(\sigma)$ transition, leading to the appearance of a lower energy charge-transfer transition with reduced intensity relative to the $^2E_u(\sigma)$ charge-transfer transition in the absorption spectrum in Figure 2b.

Having experimentally assigned the ligand-field and charge-transfer excited-state spectrum in the 10 000–45 000-cm^{-1} region which contains the transitions from all the valence orbitals in Figure 2a, one can now evaluate the performance of the SCF-Xα-SW calculations in describing the bonding in D_{4h}-$CuCl_4^{2-}$ over a large energy region.[16] The results of a transition-state Xα calculation[17] using the Norman sphere radii are presented at the bottom of Figure 2b. Comparison to the experimental spectra shows that the d→d transitions are too high in energy and the charge-transfer transitions are too low, consistent with the ground-state results, indicating that this calculation generates a description of the bonding which is too covalent (i.e., the metal and ligand orbitals are too close in energy). However, the results of the SCF-Xα-SW calculation adjusted to the ground-state EPR data (Figure 2b, bottom) provide extremely good agreement between predicted and observed ligand-field and charge-transfer excited-state energies, again indicating that the bonding in this tetragonal cupric model complex is well described by this level of electronic structure calculation.

To summarize: a normal cupric complex is expected to have a tetragonal geometry with a $d_{x^2-y^2}$ ground state which exhibits an EPR signal with $g_\parallel > g_\perp > 2.0023$ and a large parallel hyperfine splitting ($A_\parallel > 140 \times 10^{-4}$ cm^{-1}). Weak ligand-field excited states ($\epsilon < 50$ M^{-1} cm^{-1}) are expected in the 550–800-nm region and intense ligand-to-metal charge-transfer transitions dominate the higher energy region (the energy being dependent on the valence ionization energy of the specific ligand). There should be both σ- and π-charge-transfer transitions with the σ at higher energy with greater intensity due to its greater overlap with the $d_{x^2-y^2}$ orbital.

III. Blue Copper Proteins

The absorption and EPR spectra of the blue copper site in plastocyanin are given in Figure 3, a and b.

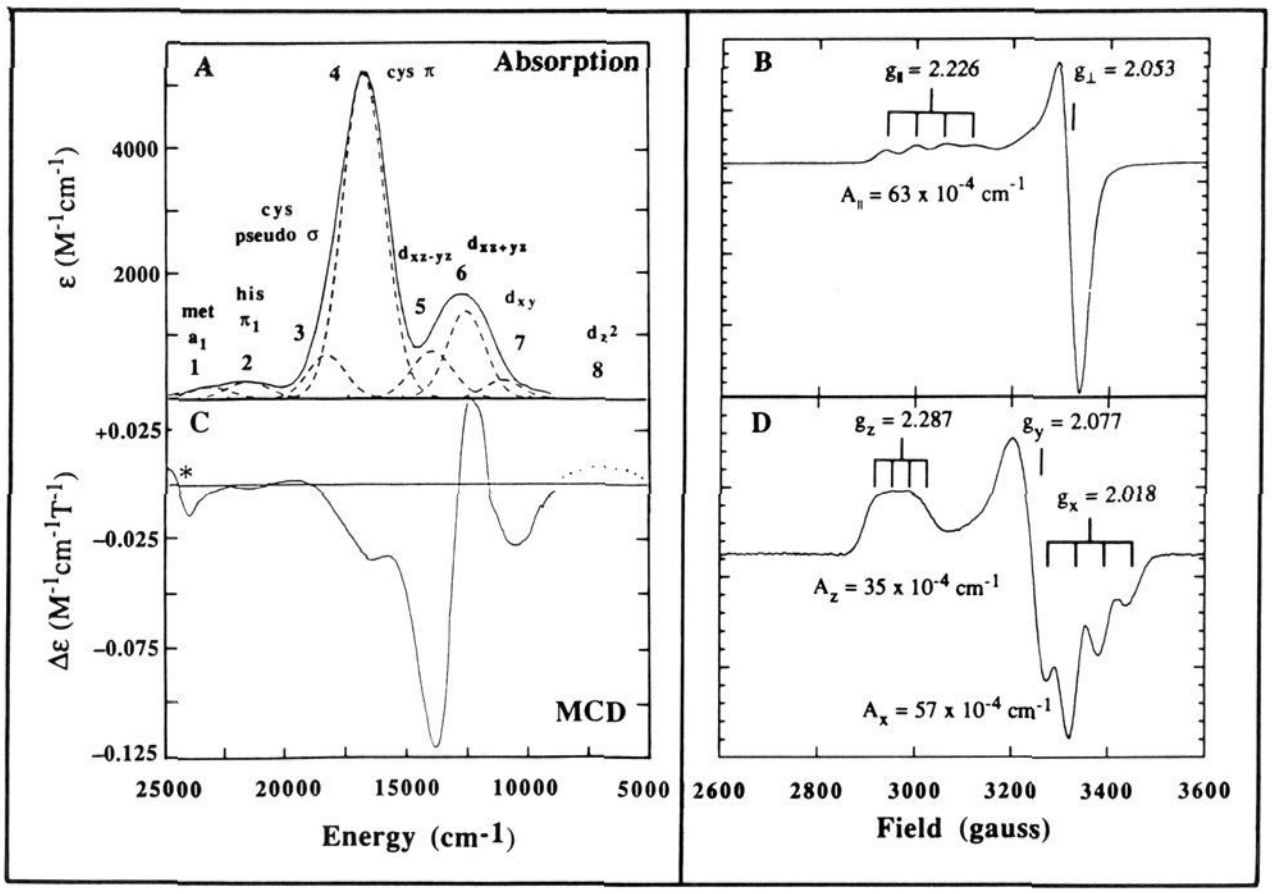

Figure 3. *Unique spectral features of blue copper proteins: Part A shows the low-temperature (LT) absorption spectrum of plastocyanin.* The dashed lines indicate Gaussian band deconvolution of the spectrum. Assignments of bands 1–8 were determined from LT-absorption and LT-MCD spectroscopies. Part B shows the EPR spectrum of spinach plastocyanin, and C, the LTMCD spectrum of spinach plastocyanin. The dotted portion of the spectrum is estimated from the NIR-LT-MCD spectrum of azurin (see ref 26). The feature marked with an asterisk (*) is due to a small amount of heme impurity. Part D shows the EPR spectrum of stellacyanin.

These are clearly different from the spectra of a normal cupric complex shown in Figures 1d and 2. As seen in the EPR spectrum, $g_{\parallel} > g_{\perp} > 2.0023$, which indicates that the blue copper site has a $d_{x^2-y^2}$ ground state. However, the parallel hyperfine splitting is very small ($A_{\parallel} = 63 \times 10^{-4}$ cm^{-1}).[18] In the absorption spectrum, instead of weak ligand-field transitions, the blue copper site exhibits an intense band ($\epsilon \approx 5000$ M^{-1} cm^{-1}) at ~600 nm. These features were interpreted as suggesting that the blue copper site had a distorted tetrahedral rather than tetragonal geometry with a thiolate sulfur from a cysteine residue bound to the copper producing a low-energy ligand-to-metal charge-transfer transition which corresponds to the 600-nm band in Figure 3a.[19] In 1978, Freeman, et al.[20] published the X-ray structure of plastocyanin (Figure 4), which confirmed the above model and identified the remaining three ligands as two nitrogens of imidazole rings of histidine residues and a thioether sulfur of methionine which has a quite long 2.9-Å Cu–S bond length. The structures of several azurins have now also been reported.[21,22] Consistent with the fact that their spectral features are similar to those of plastocyanin, the azurins have basically the same active site structure as in Figure 4, but with an additional carbonyl oxygen of the protein backbone at a 3.1-Å distance from the copper, trans to the thioether sulfur[22] (vide infra). Stellacyanin has no methionine in its sequence and exhibits a perturbed blue copper EPR spectrum as shown in Figure 3d.[23] This spectrum differs from that of plastocyanin in Figure 3b due to a rhombic splitting of $g_{\perp}$ (i.e. $g_x \neq g_y$) and a fairly sizable hyperfine splitting in the $g_{\perp}$ region. While no crystallographic information is available on stellacyanin, ligand-field theory indicates that the above spectral differences derive from some mixing of d_{z^2} (~5%) into the $d_{x^2-y^2}$ ground state.[9] Structurally, this mixing would occur if the thioether sulfur in plastocyanin were replaced with a stronger field ligand in stellacyanin. Recent pulsed ENDOR data do in fact indicate that a deprotonated amide nitrogen binds to the copper site in stellacyanin at high pH.[24]

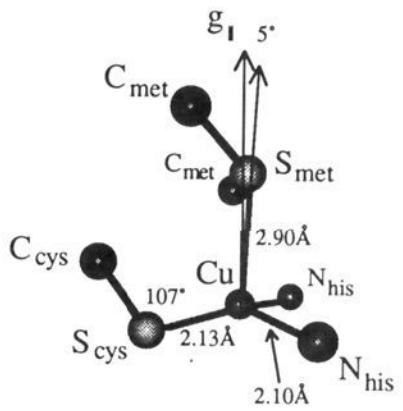

Figure 4. X-ray structure of the copper coordination environment of oxidized poplar plastocyanin at 1.6-Å resolution.[20] The $g_{\parallel}$ orientation was determined from single-crystal EPR spectroscopy.[25]

A combination of polarized single-crystal electronic absorption, single-crystal EPR, single-crystal X-ray absorption, low-temperature magnetic circular dichroism (LTMCD), and SCF-Xα-SW calculations have been used to define in detail the nature of the unusual ligand–metal bonding interactions at this active site, and the nature of the ground-state wave function which plays the key role in the electron-transfer reactivity.[13,25–27]

A. Nature of the Ligand–Metal Bonding Interactions

The thiolate-copper bond dominates the electronic structure of the blue copper active site. The electronic contributions to this bond are given in Figure 5 which shows the Xα-calculated contours of the valence-orbital wave functions of a free thiolate ligand (left) and the

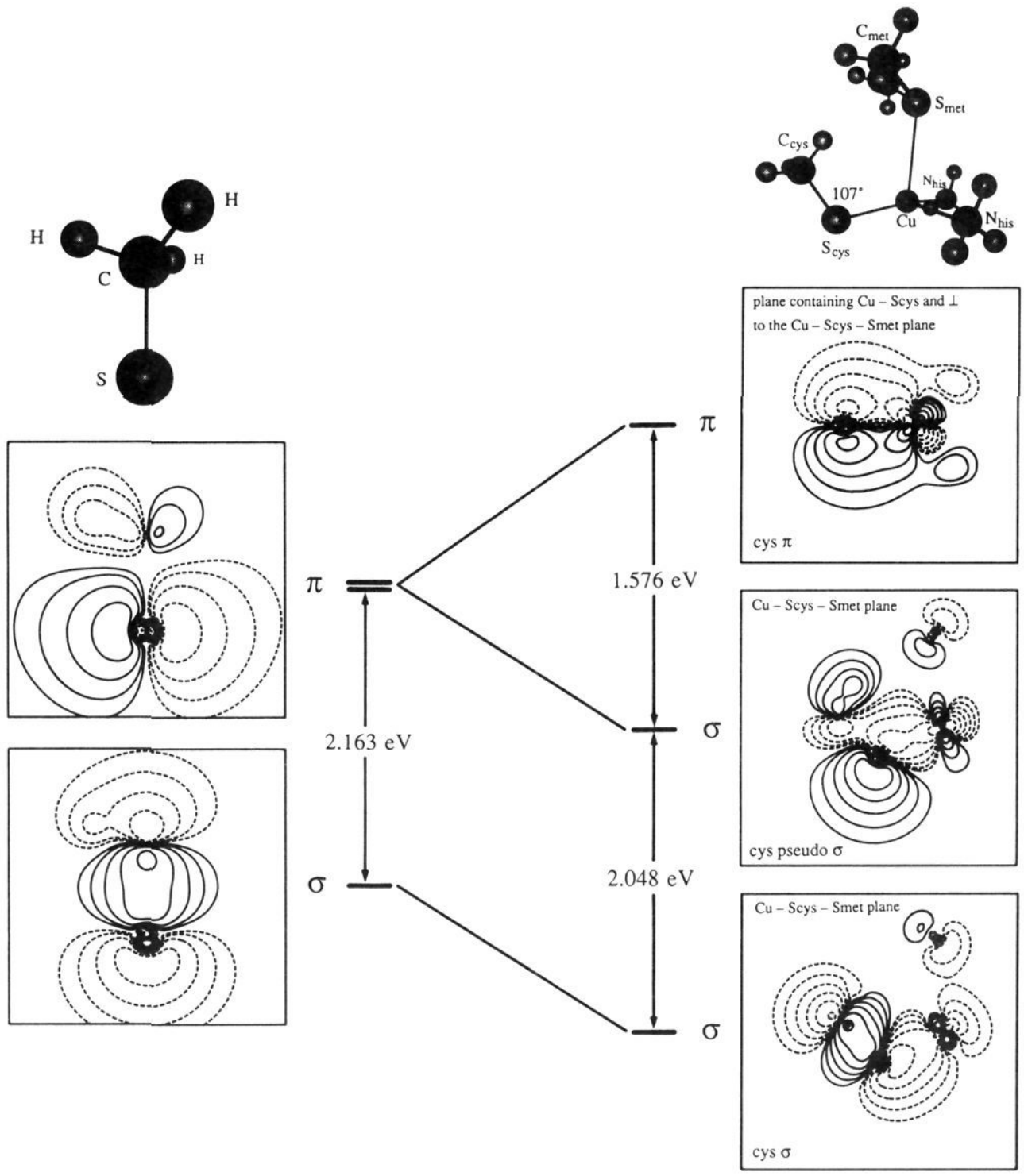

Figure 5. The thiolate–copper bond. The approximated blue copper site used in the SCF-Xα-SW calculations has methyl thiolate (SCH_3^-) substituted for cysteine, dimethyl thioether $S(CH_3)_2$ for methionine, and ammonia (NH_3) for the imidazole rings of the histidine residues.[13] The ammonia and dimethyl thioether groups have been slightly shifted to give the model C_s symmetry. [Note that SCF-Xα-SW calculations using the crystallographic coordinates (C_1 symmetry) show no systematic changes.[13]] The left-hand side of the figure shows the SCF-Xα-SW wave function contours for the highest occupied orbitals of methyl thiolate. The right-hand side gives the contours for the π, pseudo-σ, and σ-bonds the thiolate forms upon bonding to the blue copper site. The projection shown for the π orbital contains the Cu and S_{cys} atoms and is perpendicular to the Cu–S_{cys}–C_{cys} plane (i.e. out of the plane of the paper for the model as shown). The two σ-orbital wave function contours are projected from the plane defined by the Cu–S_{cys}–C_{cys} atoms and have the same orientation as the molecule shown above the contour diagrams. Contour lines for all figures are at ±0.64, ±0.32, ±0.16, ±0.08, ±0.04, and ±0.02 $(\text{electrons/bohr}^3)^{1/2}$.

effects on these of bonding to the copper center (right) with the geometry fixed at that of the plastocyanin crystal structure[20] in Figure 4. Of particular importance here is the bent C–S–Cu bond angle of 107°. The highest occupied orbitals in free thiolate are a doubly degenerate π set which are mostly S 3p orbitals perpendicular to the carbon–sulfur bond. To deeper binding energy is the third S 3p orbital which is σ bonding to the methyl group. Upon binding to the copper with the 107° angle, these orbitals split into three nondegenerate levels. The highest energy orbital is oriented perpendicular to the C–S–Cu plane and is thus π bonding to the copper, and the deepest binding energy thiolate valence orbital is now a σ bonding molecular orbital having mostly S–C character but delocalized over the C–S–Cu framework. It is important to note that the remaining π level of the free ligand, the S 3p orbital which is the C–S–Cu plane of the complex, has the contour shown in the middle of Figure 5, indicating that its electron density lies mostly along the S–Cu bond and has become σ bonding to the copper (i.e. the pseudo σ level).[13] Thus we find that the thiolate–copper bond has one π and two σ interactions (rather than two π and one σ interaction which would normally be expected for a ligand–metal bond), and this unusual electronic structure occurs because of the orientation of the thiolate at the copper center. This orientation can be strongly regulated by the covalent linkage of this residue into the protein chain.

There has been some discussion as to whether there is a bonding interaction between copper and the thioether sulfur at 2.9 Å in plastocyanin[28] and whether the azurins should be viewed as five-coordinate trigonal bipyramidal sites due to the additional interaction with the carbonyl oxygen at 3.1 Å.[22] The contours of the valence orbitals of these ligands which would be in-

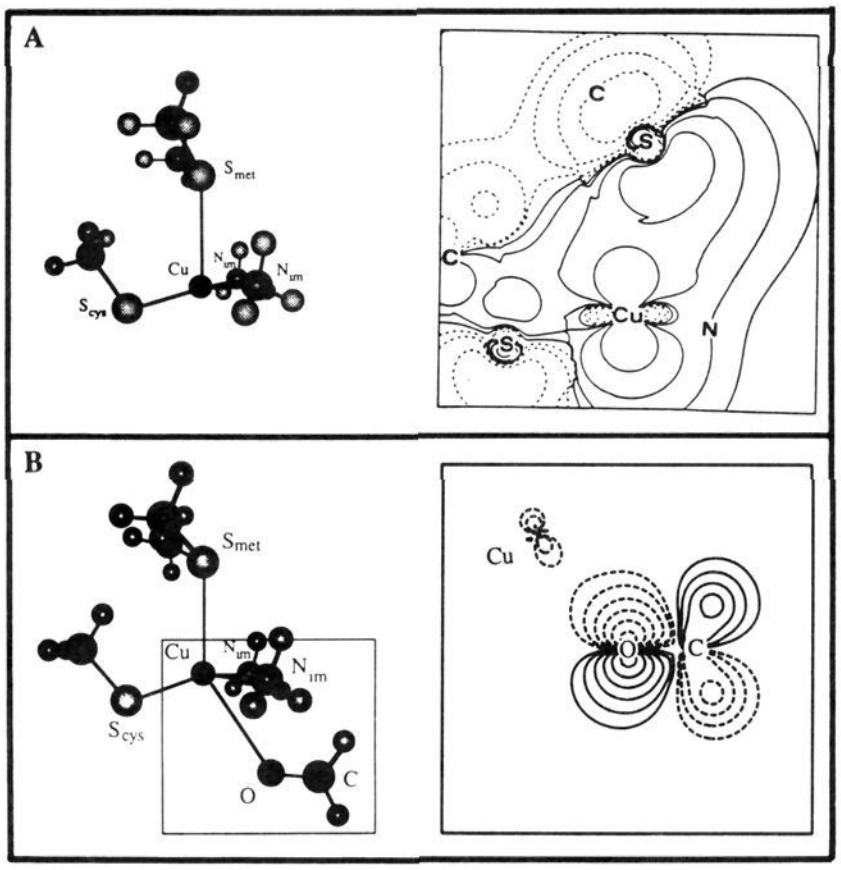

Figure 6. The thioether–copper bond and carbonyl oxygen–copper interaction: Part A shows SCF-Xα-SW wave function contour plot of the thioether–copper bond (2.901 Å) from ref 13; the wave function is projected in the S_{met}–Cu–S_{cys} plane. The orientation of the model used in the calculation is shown to the left. Part B shows the formaldehyde HOMO orbital–copper interaction (Cu–O distance = 3.12 Å, Cu–O–C (formaldehyde) angle = 128°).[22d] The area in the frame is expanded in the contour plot shown at the right which contains the Cu and formaldehyde O and C atoms. The formaldehyde HOMO has <1% Cu character.

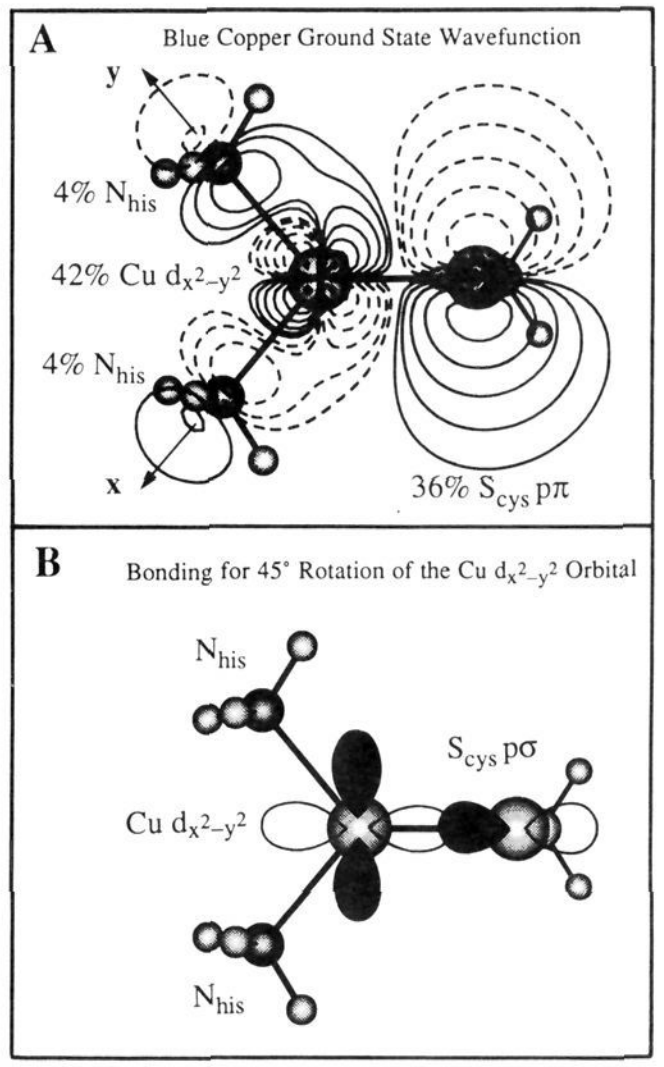

Figure 7. Possible thiolate-copper bonding interactions: (A) bonding mode with the $d_{x^2-y^2}$ orbital involved in a π-bonding interaction with the cysteine sulfur; and (B) bonding scheme with the $d_{x^2-y^2}$ orbital rotated 45° so as to σ bond to the cysteine sulfur.

volved in bonding to the copper are given in Figure 6. From Figure 6a the thioether does undergo a bonding interaction with the copper center. This involves the thioether a_1 molecular orbital, a mostly S 3p orbital in the molecular plane pointing out the sulfur end of the thioether, which undergoes a σ-bonding interaction with the d_{z^2} orbital on the copper. It should be noted that as both the thioether a_1 and the copper d_{z^2} orbitals are filled, there should be no net bonding; however, about 5% Cu 4s and 4p is mixed into the thioether a_1 level which generates a weak covalent bond. In contrast, the carbonyl oxygen valence orbital acquires very little (<1% d_{z^2}, 4s, 4p) copper character at 3.1 Å, indicating no net bond.[29] This reflects the large difference in the radial distribution function of a carbonyl 2p oxygen as compared to a thioether 3p sulfur orbital.

B. Nature of the Ground-State Wave Function

The oxidized blue copper center has a half-occupied $d_{x^2-y^2}$ orbital which accepts and transfers electrons in the redox reactivity of this site. The determination of its orientation with respect to the geometric structure in Figure 4 and its covalent delocalization onto the ligands is of critical importance in understanding the functioning of this site in long-range electron transfer to specific locations on or in the protein. Single-crystal EPR studies on plastocyanin have shown[25] that $g_\parallel$ is oriented approximately along the long thioether S–Cu bond (Figure 4) which fixes the $d_{x^2-y^2}$ orbital perpendicular to this direction and within 15° of the plane defined by the three strong, thiolate S and imidazole N ligands. Comparison of the low-temperature MCD data in Figure 3c with the absorption data in Figure 3a indicates that bands 5–8, which are relatively weak in absorption, are intense in the low-temperature MCD spectrum, allowing these to be identified as d→d transitions.[26] These NIR ligand-field transitions are characteristic of blue copper centers and are not present in the spectra of normal copper complexes. The specific ligand-field excited-state assignments indicated at the top of the bands in Figure 3a are based on the MCD signs and magnitudes. The d orbital splitting pattern obtained, x^2-y^2 (ground state) > z^2 > xy > $(xz + yz)$ > $(xz - yz)$, reflects a rhombically distorted, elongated C_{3v} effective symmetry for the blue copper site in Figure 4. The z (i.e., C_3) axis corresponds to the long Cu–S (thioether) bond consistent with the EPR results. The rhombic interaction derives from the strong thiolate-Sp π interaction with the copper (vide infra, adjusted SCF-Xα-SW calculations) which raises the energy of the $d_{x^2-y^2}$ orbital relative to the d_{xy} level (which are degenerate in C_{3v}) and thus orients the highest energy half-occupied orbital of the blue copper site such that its lobes bisect the thiolate S–Cu bond as shown in Figure 7a.

This C_{3v} effective symmetry raised a major problem with respect to the generally accepted explanation[30] for the small parallel hyperfine splittings found in the EPR spectra of some copper complexes. As with the blue copper site in Figure 3b, $CuCl_4^{2-}$ distorted toward a flattened tetrahedral structure also exhibits a small $A_\parallel$ value. This complex has D_{2d} symmetry, and Bates and Stevens[31] have shown that in this symmetry the Cu $4p_z$ orbital can mix into the $d_{x^2-y^2}$ level and that this will reduce the value of $A_\parallel$. There are three contributions to the hyperfine splitting: Fermi contact, spin dipolar, and orbital dipolar. The spin dipolar contribution of

a p_z orbital is opposite to that of a $d_{x^2-y^2}$ orbital. Approximately 12% $4p_z$ mixing into the $d_{x^2-y^2}$ orbital will reduce a normal hyperfine splitting to that of D_{2d}-$CuCl_4^{2-}$ or the blue copper sites.[30] However, for the effective C_{3v} symmetry of the blue copper site, the $d_{x^2-y^2}$ ground state can only mix with the Cu $4p_x,p_y$ levels which will increase, not decrease the $A_\parallel$ value. X-ray absorption spectroscopy (XAS) was used to probe the Cu $1s \rightarrow 3d_{x^2-y^2}$ transition at 8979 eV, which gains intensity from Cu 4p mixing. Single-crystal XAS studies show that this transition in plastocyanin is polarized perpendicular to the thioether S–Cu bond (i.e., it is x,y polarized) confirming that only $4p_x,p_y$ are mixed into the $d_{x^2-y^2}$ level.[27] This is important because it eliminates $4p_z$ mixing as the explanation for the small hyperfine splitting in the blue copper site and allows one to focus on covalency as the origin of the reduction in the hyperfine interaction. Delocalization of the unpaired electron onto the ligands reduces the electron spin's interaction with the copper nuclear spin. We have quantitatively evaluated the effects of covalency on the $d_{x^2-y^2}$ orbital through SCF-Xα-SW calculations adjusted to the ground-state data[13,26] as described above for D_{4h}-$CuCl_4^{2-}$. These calculations show that this half-occupied orbital is highly covalent (only ~42% Cu $d_{x^2-y^2}$ character) and that, in contrast to D_{4h}-$CuCl_4^{2-}$ in Figure 1e, this covalency is highly anisotropic with about half the wave function delocalized onto the S p π orbital of the thiolate ligand (Figure 7a).

This orientation and anisotropic delocalization of the ground state of the blue copper site might be expected to play an important role in defining electron-transfer pathways, particularly if a through-bond superexchange mechanism[32] is active. A beautiful example where this is likely the case is the intramolecular electron transfer in the multicopper oxidases. We have shown that the type 2 and type 3 centers together form a trinuclear copper cluster which is the site of reduction of dioxygen to water[33] (see section V). Crystallographic results have recently appeared on ascorbate oxidase[34] which show that the type 1 copper is very similar to the blue copper site in plastocyanin and that it is 12.2 Å from the two type 3's of the trinuclear copper cluster. The type 1 copper must rapidly transfer electrons over this distance to the trinuclear copper cluster during catalysis. The thiolate ligand of the type 1 center is covalently bound on both sides in the protein primary structure to histidines which are ligands to the two type 3 coppers of the trinuclear copper cluster. This type of cysteine–histidine intramolecular protein connection between a blue copper site and an additional copper is also found in the crystal structure of nitrite reductase.[35] We have superimposed the ground-state wave function obtained from the SCF-Xα-SW calculations for the blue copper site on the type 1 center in ascorbate oxidase in Figure 8. The orientation and anisotropic delocalization of the redox-active orbital of the blue copper site into the thiolate[36] clearly favors a through-bond covalent protein pathway to the trinuclear copper cluster and suggests that the metal ion's electronic structure makes a significant contribution to intramolecular long-range electron transfer in the multicopper oxidases.

A final point should be made with respect to a possible hole superexchange mechanism for the reduction of the oxidized blue copper site. This would involve a low-energy, intense ligand-to-metal charge-transfer transition, and the dominant band 4 in Figure 3a, which is responsible for the unique absorption spectrum of the blue copper site, is in fact assigned as the thiolate $\pi \rightarrow$ Cu(II) charge transfer transition. As mentioned earlier, one normally expects the π charge transfer transition to be weak due to poor overlap. This assumes that the $d_{x^2-y^2}$ orbital has one of its lobes oriented along the ligand–metal bond as is normally the case (Figure 7b). However, as indicated above, the thiolate π interaction with the copper is very strong and rotates the $d_{x^2-y^2}$ orbital by 45° (Figure 7a), thus providing a very efficient π-superexchange mechanism through the thiolate ligand of the blue copper site.

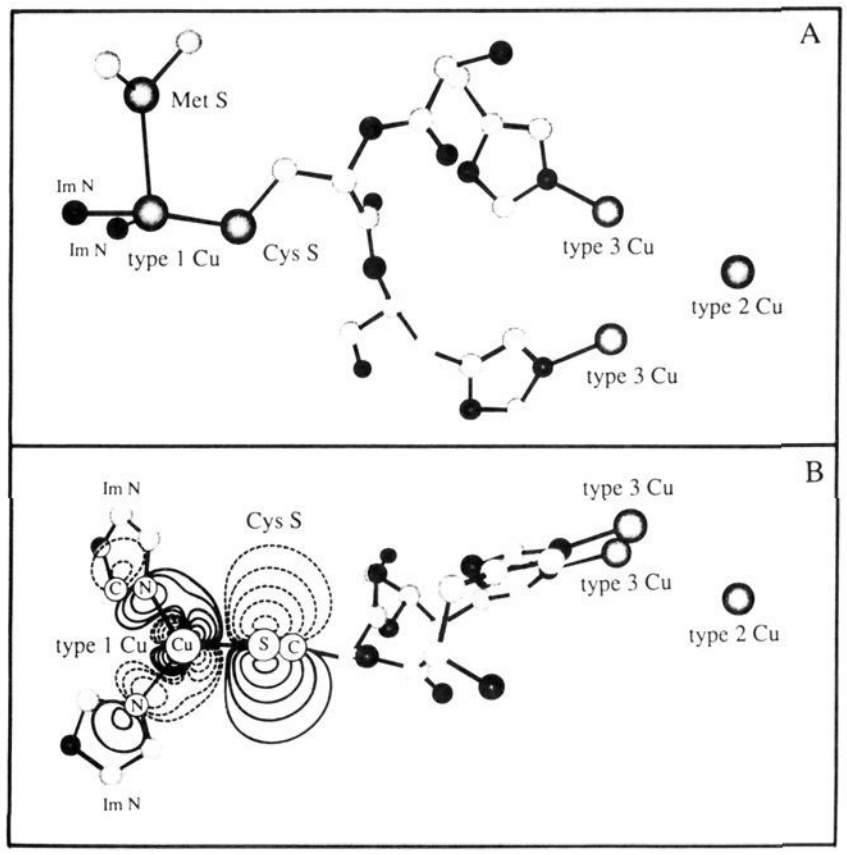

Figure 8. Proposed electron transfer pathway in ascorbate oxidase.[34] Part A is a view of the copper centers in ascorbate oxidase viewed in the methionine sulfur (Met S), type 1 copper, cysteine sulfur (S cys) plane. For clarity, only the peptide backbone atoms connecting the type 1 and type 3 copper centers are included. Part B is a view normal to the Met S–Cu bond (with the Met S group omitted for clarity) with the plastocyanin ground-state HOMO wave function contour superimposed on the type 1 copper site. Contour lines are at ±0.64, ±0.32, ±0.16, ±0.08, and ±0.04 (electrons/bohr^3)$^{1/2}$.

IV. Coupled Binuclear Copper Proteins

Deoxyhemocyanin contains a binuclear cuprous site which binds dioxygen as peroxide, producing oxyhemocyanin. The two coppers in oxyhemocyanin are electronically coupled in that both are in the cupric oxidation state (from XAS studies)[37] yet this site exhibits no EPR signal. Magnetic susceptibility studies[38] show that this derives from a strong antiferromagnetic coupling between the two Cu(II) to form $S_{total} = 0$ and 1 states with the triplet higher in energy than the singlet by >600 cm^{-1}. This large antiferromagnetic coupling requires orbital overlap between the two Cu(II) and since EXAFS indicates that the coppers are ~3.6 Å apart,[37] this must involve a superexchange pathway through a bridging ligand. Results from crystallography are currently available to 3.2-Å resolution only for the deoxy site[39] which show that each copper has three histidine ligands but no bridging ligand. Thus the superexchange pathway must be formed on binding dioxygen and oxidizing the site.

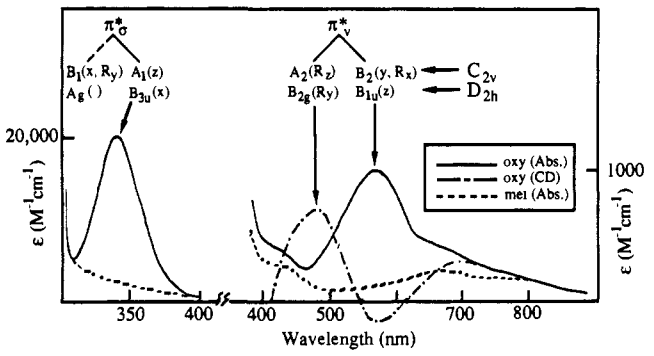

Figure 9. Electronic spectra of oxyhemocyanin: absorption and CD spectra of oxyhemocyanin and absorption spectrum of met hemocyanin, with assignments and selection rules for peroxide-to-copper charge transfer transitions (indicated by arrows) in the C_{2v} and D_{2h} dimer geometries.

Since the strong antiferromagnetic coupling in the ground state makes it spectroscopically inaccessible, spectral studies have focused on the unique excited state features of oxyhemocyanin (Figure 9). The absorption spectrum shows two bands, one at ~580 nm with $\epsilon \sim 1000\ M^{-1}\ cm^{-1}$ and an extremely intense transition at ~350 nm, $\epsilon \sim 20000\ M^{-1}\ cm^{-1}$. In the CD spectrum, there is an additional positive band at 480 nm which has no counterpart in the absorption spectrum. These unusual excited state spectral features are now well understood and define the geometric and electronic structure of this active site. Correlation to tyrosinase has further provided important insight into electronic contributions to the activation of dioxygen by this monooxygenase.

A. Origin of Excited-State Spectral Features

Displacement of peroxide from oxyhemocyanin results in a binuclear cupric site known as the met derivative.[40] As shown in Figure 9, this form only exhibits weak d→d transitions at ~700 nm, characteristic of tetragonal Cu(II). Magnetic susceptibility studies show that the met derivative is also strongly antiferromagnetically coupled and thus must contain a bridging ligand.[41] On the basis of the deoxyhemocyanin crystal structure, this endogenous bridge is likely to be hydroxide from water. The 350- and 580-nm absorption and 480-nm CD bands of oxyhemocyanin are not present in the met derivative allowing these to be assigned as peroxide-to-Cu(II) charge transfer transitions.

The highest occupied valence orbitals of peroxide are the π^*-degenerate set which splits on binding to the copper (Figure 10a). The π^*_σ orbital is oriented along the Cu–O bond and has significant σ overlap with the Cu(II) $d_{x^2-y^2}$ orbital. Excitation from this orbital gives rise to a high-energy intense O_2^{2-} π^*_σ→Cu(II) $d_{x^2-y^2}$ charge-transfer transition. The π^*_υ level is vertical to the Cu–O bond and π bonding to the copper. Excitation from this orbital is expected to result in a O_2^{2-} π^*_υ→Cu(II) $d_{x^2-y^2}$ charge-transfer transition at lower energy and with lower intensity than the π^*_σ-charge-transfer transition. Karlin has synthesized a model complex[42] which has been shown by resonance Raman studies to bind dioxygen as peroxide to a single Cu(II) center.[43] This complex exhibits (Figure 10b) an O_2^{2-}→Cu(II) charge-transfer absorption spectrum which is as predicted in Figure 10a. The spectrum in Figure 10b is, however, very different from that of oxyhemocyanin (Figure 9) in that the O_2^{2-} π^*_σ→Cu(II) charge transfer band is more intense and at higher energy in oxyhemocyanin (the 350 nm band), and the π^*_υ region in Figure 9 exhibits two bands, one in absorption and one only in the CD spectrum.

These spectral differences derive from bridging the peroxide between the two Cu(II). Overlap with a second Cu(II) stabilizes the π^*_σ orbital, raising the π^*_σ→Cu(II) charge-transfer energy and increasing its intensity. Further, each charge-transfer transition of a monomer in Figure 10a should split into four possible charge-transfer transitions in a peroxide-bridged dimer (Figure 10c).[44-46] Just as in the ground state, the unpaired electron in a charge-transfer excited state should undergo an antiferromagnetic coupling with the second Cu(II) producing an excited-state singlet/triplet splitting which can be much larger than in the ground state.[47] Since the antiferromagnetic ground state is a singlet, only spin-allowed transitions to the singlet excited states should have significant absorption intensity. The singlet (and triplet) state will undergo an additional splitting (a transition dipole vector coupling (TDVC)) into two states which correspond to the symmetric and antisymmetric combinations of O_2^{2-}→Cu(II) charge-transfer transitions to the two coppers of the dimer. This TDVC splitting of the singlet reflects the transfer of the charge-transfer excitation between the two halves of the dimer and can be related to the HOMO/LUMO splitting of the $d_{x^2-y^2}$ orbitals of the two Cu(II).[48] This dimer splitting of a ligand-to-metal charge-transfer transition has, in fact, been observed[45] in copper azide model complexes.[49] From Figure 10d, N_3^- bound to a single Cu(II) produces one π_σ→Cu(II) charge-transfer transition at ~400 nm. This transition splits into two absorption bands on going to the cis-μ-1,3 azide-bridged model complex. Finally, as shown at the bottom of Figure 10d, binding N_3^- to met hemocyanin produces a charge-transfer spectrum very similar to that of the cis-μ-1,3 model complex, indicating a similar spectroscopically effective model for the active site in this derivative.

The high energy and intensity of the π^*_σ→Cu(II) charge-transfer transition and the presence of three charge transfer bands in Figure 9 require that peroxide bridge the two Cu(II) in oxyhemocyanin.[40] Of the possible end-on peroxide-bridged structures (cis- and trans-μ-1,2 and -μ-1,1) only the cis-μ-1,2 structure (Figure 11, top left) could produce spectral features consistent with those of oxyhemocyanin. This structure would derive from the met N_3^- model in Figure 10d by replacing the cis-μ-1,3 N_3^- with a μ-1,2 peroxide. Thus far end-on complexes with trans-μ-1,2 and -μ-1,1 peroxide-bridged structures have been obtained by Karlin[50] and indeed their spectral features are very different from those of oxyhemocyanin. Recently, Kitajima[51] has structurally defined the first side-on peroxide bridge (μ-η^2:η^2) in a transition metal complex (Figure 11, top right). There has been some discussion with respect to the spectral features associated with this complex in solution,[52-54] however, data have now been obtained on crystalline material[55] which show spectral features very similar to those of oxyhemocyanin.

The cis-μ-1,2 structure has C_{2v} symmetry and the μ-η^2:η^2 geometry has D_{2h} dimer symmetry. As indicated

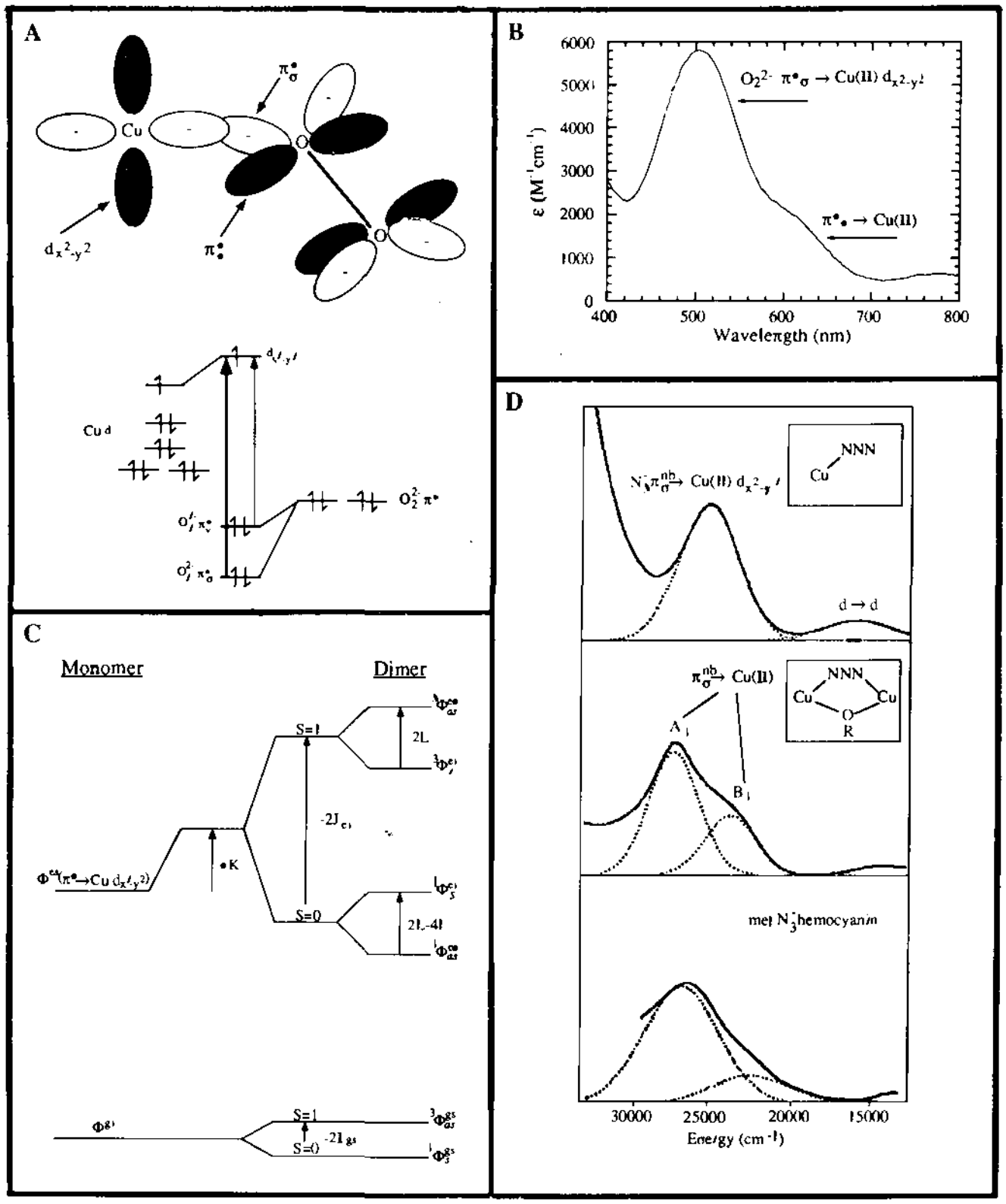

Figure 10. Charge-transfer transitions in copper monomers and dimers. Part A shows orbital interactions involved in peroxide–copper bonding and charge transfer transitions (arrow thickness indicates predicted relative absorption intensity). Part B shows charge-transfer absorption spectrum of peroxide bound to a single Cu(II). Part C shows ground-state and charge-transfer excited-state splittings due to dimer interactions in a peroxide-bridged copper dimer. ($^1\Phi_s^{es}$) is the symmetric singlet excited state, etc. K is the additional coulomb interaction in the dimer, J_{es} is the excited-state magnetic exchange, and I and L are the coulomb and exchange contributions to excitation transfer between the two halves of the dimer which result in the symmetric/antisymmetric splitting. Part D shows azide-to-copper charge-transfer features in the absorption spectrum of model complexes with azide bound to one copper (top), azide-bridged (cis-μ-1,3) copper dimers (middle), and met azide hemocyanin (bottom).

at the top of Figure 9, each monomer $O_2^{2-}\rightarrow$Cu(II) charge-transfer transition should split into two singlet states in the dimer with the orbital symmetry and selection rules derived from the TDVC model as indicated. There are two important results to emphasize here. First, for both possible structures the π^*_v splits into one transition which is electric dipole allowed and therefore present in the absorption spectrum and a second transition which is only magnetic dipole allowed and therefore should have significant intensity only in the CD spectrum, explaining the origin of the 480-nm CD band. Second, the intense component of the π^*_σ charge-transfer transition (i.e. the 350-nm band) is predicted to have different polarizations for the two structures. In the cis-μ-1,2 structure, it should be polarized perpendicular to the Cu–Cu axis, while in the μ-η^2:η^2-structure it is polarized along the Cu-Cu vector. Thus, while the existing data favor the side-on bridging structure on the basis of its spectral similarities to oxyhemocyanin, these two structures can be unambiguously distinguished through correlation of polarized single-crystal spectral studies on the oxyprotein active site with the X-ray crystallography of the site, both of which are currently in progress.[56,57]

B. Electronic Structure of Oxyhemocyanin

The electronic structures of the cis-μ-1,2 and μ-η^2:η^2 peroxide-bridged binuclear copper model geometries (Figure 11, top) have been defined through broken-symmetry SCF-Xα-SW calculations which have been calibrated through comparison to spectral data.[58] Spin-unrestricted broken-symmetry Xα-SW calculations have been shown to provide reasonable bonding

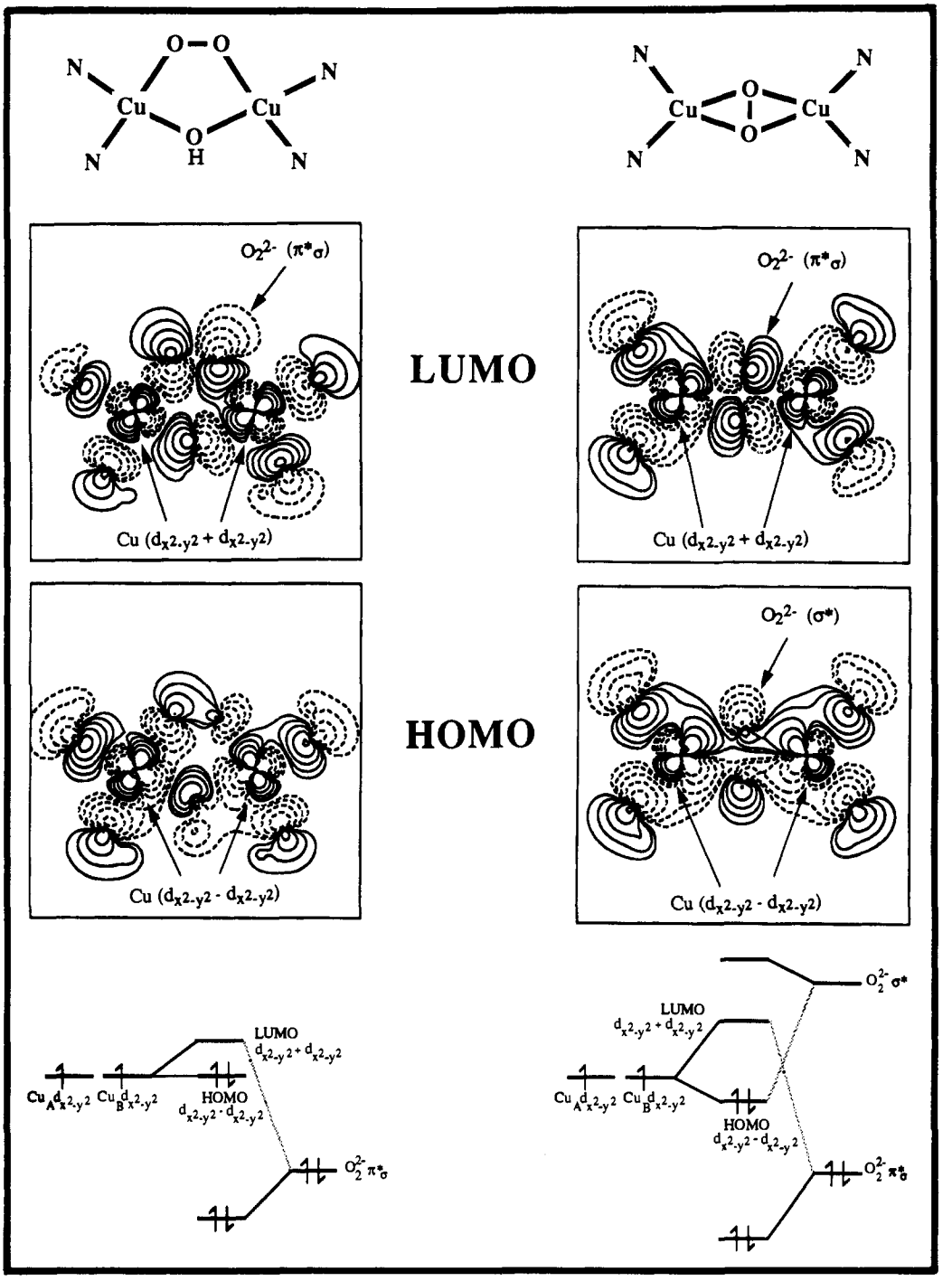

Figure 11. Geometric and electronic structures for end-on cis-μ-1,2 (C_{2v}) and side-on μ-η^2:η^2 (D_{2h}) models of the oxyhemocyanin active site: top, geometric structures; center, contours of the HOMO and LUMO orbitals of each from broken-symmetry SCF-Xα-SW calculations; bottom, energy-level diagrams showing dominant orbital contributions. (Cu_A and Cu_B refer to each of the two coppers in the dimer.)

descriptions for antiferromagnetically coupled binuclear metal complexes based on the multideterminant nature of the broken-symmetry state.[59] In the broken-symmetry calculation the full molecular symmetry is lowered to C_s(cis-μ-1,2) or C_{2v}(μ-η^2:η^2) and equal but opposite up-down spin symmetry is imposed on the two halves of the dimer. Thus each broken symmetry state can be partially localized onto one-half of the dimer and each spin-up level is degenerate with a spin-down level on the opposite side of the molecule. The key features of the peroxide–copper bond are given by the energies and wave functions of the HOMO and LUMO levels of each complex, which are dominantly metal centered and involve the peroxide valence orbital interactions with the symmetric (LUMO) and antisymmetric (HOMO) combination of $d_{x^2-y^2}$ orbitals on the two Cu(II). From Figure 11, the dominant interaction in the cis-μ-1,2 structure is as qualitatively described above for an end-on peroxide-copper bond in Figure 10a. The LUMO of the end-on bridged dimer is raised in energy due to its antibonding interaction with the O_2^{2-}-π^*_σ orbital which is involved in an electron-donor interaction with the metal centers. The HOMO is relatively nonbonding with respect to the peroxide. For the side-on bridged structure in Figure 11, the dominant interaction again involves the O_2^{2-}-π^*_σ-level destabilizing

the symmetric combination of $d_{x^2-y^2}$ orbitals on the two Cu(II). It should be noted in Figure 11 that this σ-donor interaction with the LUMO is considerably larger than in the end-on bridged structure. This reflects the fact that the side-on bridged O_2^{2-} should be viewed as occupying two coordination positions on each Cu(II) and each involves a π^*_σ-donor interaction. In addition, for the side-on bridged structure these Xα calculations provide a new bonding description for peroxide. The HOMO is found to be stabilized in energy indicating that *the peroxide is acting as a π-acceptor ligand.* From the HOMO contour in Figure 11 (right), this energy level is stabilized through a bonding interaction with the high-energy σ^* orbital of the peroxide. This is only found to occur for the side-on bridged structure. Thus, relative to the end-on bridged structure, the side-on bridging peroxide undergoes both a stronger σ-donor and an additional π-acceptor interaction. Together these lead to a stronger copper–peroxide bond for the side-on bridge which should contribute to the relative abilities of these two geometries to reversibly bind dioxygen.

These electronic structure descriptions also provide important insight into the physical properties of these two model structures. The HOMO/LUMO splitting directly relates to the magnitude of the antiferromagnetic coupling of the binuclear cupric site.[60] This splitting is larger in the side-on bridged structure, indicating that it should exhibit the largest singlet/triplet splitting in the ground state. Thus peroxide bridging in this mode provides a very effective superexchange pathway. It should be noted that the cis structure also contains an OH^- bridge which interacts with the LUMO and contributes to the antiferromagnetic coupling in this structure. The stronger O_2^{2-} π^*_σ-donor interaction with the $d_{x^2-y^2}$ orbitals on the coppers in the side-on structure indicates that this level is more stabilized in energy and has greater ligand–metal overlap. Thus its O_2^{2-} $\pi^*_\sigma \rightarrow$Cu(II) charge-transfer transition should be considerably higher in energy and more intense than in the cis structure. Xα calculations show that the O_2^{2-} π^*_σ interactions in the cis- and trans-μ-1,2 structures are very similar. The O_2^{2-} $\pi^*_\sigma \rightarrow$Cu(II) charge-transfer transition has been studied in the structurally defined trans complex,[46] and it is considerably lower in energy and weaker than the 350-nm π^*_σ-charge-transfer band in oxyhemocyanin. Thus the spectral features in Figure 9 require a stronger O_2^{2-} π^*_σ-donor interaction in oxyhemocyanin as is present in the side-on bridged model geometry. Finally, oxyhemocyanin exhibits an extremely low O–O vibrational frequency of $\sim$750 cm^{-1}.[61] The intra-peroxide stretching frequency has now been measured in the monomer (800 cm^{-1}),[43] trans end-on dimer (830 cm^{-1})[46] and side-on bridged dimer (750 cm^{-1})[54-55] structures. These frequencies cannot be directly related to the O–O bond strength in that there is mechanical coupling with the Cu–O vibrations and this must be sorted out through a normal coordinate analysis. The intra-peroxide force constants obtained from normal coordinate calculations are 2.9 mdynes/Å (monomer),[43] 3.1 mdynes/Å (end-on trans dimer),[46] $\sim$ 2.5 mdynes/Å (side-on bridged dimer).[55] The increase in force constant on going from the monomer to the end-on dimer indicates a stronger O–O bond and results from the stronger π^*_σ-donor interaction which occurs upon bridging end-on to two Cu(II), each withdrawing electron density from this orbital which is π antibonding with respect to the peroxide. On going to the side-on bridged structure, the π^*_σ donor interaction is even larger indicating that the O–O bond strength should increase, in contrast to what is observed. The weakened O–O bond in the side-on bridged structure must result from the O_2^{2-} σ^*-orbital character present in the ground state HOMO.[58] While the O_2^{2-} σ^* accepts a relatively small amount of electron density from the copper, it is a strongly antibonding orbital which is extremely efficient in weakening the intra-peroxide bond.

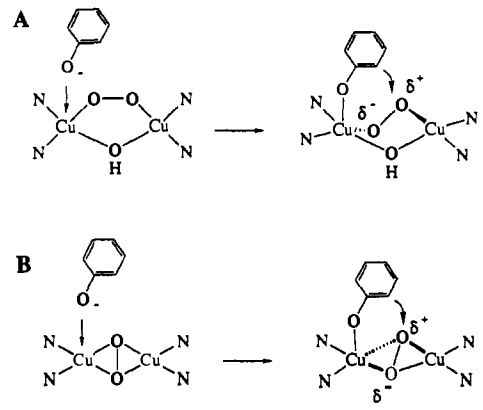

Figure 12. Proposed substrate-bound intermediates for the reaction mechanism of oxytyrosinase with both cis-μ-1,2 and μ-η^2:η^2 active site structures.

C. Molecular Mechanism of Tyrosinase

As in hemocyanin, met tyrosinase (the resting form of this enzyme) contains two Cu(II) which are antiferromagnetically coupled.[62] Met tyrosinase is reduced by reaction with *o*-diphenols to produce *o*-quinones and the deoxy site, which in turn reacts with dioxygen to produce oxytyrosinase.[63] Oxytyrosinase hydroxylates monophenols generating *o*-diphenols and the met tyrosinase site. Chemical and spectroscopic studies on a series of hemocyanin and tyrosinase active site derivatives have demonstrated that the spectroscopically effective model for the oxy site is the same in both proteins.[64] Tyrosinase has the additional feature that the site is highly accessible to substrate analogues which bind directly to a copper center.[65] This binding involves a structural rearrangement of the copper (from tetragonal to trigonal bipyramidal) which is stabilized by a strong interaction of the substrate with the protein pocket.[66] As shown in Figure 12 for both the cis-μ-1,2 and the μ-η^2:η^2 peroxide bridging structural models for oxytyrosinase, this substrate-induced rearrangement would lead to an asymmetrically coordinated peroxide. The peroxide would be heterolytically polarized with relatively more positive charge on the oxygen atom coordinated most strongly to the copper and thus activated for electrophilic attack on the phenol ring.[66,67]

For the side-on bridged structure there should be additional electronic contributions to peroxide activation. The stronger σ-donor interaction with the coppers in the side-on bridge leads to a less negative peroxide which further contributes to electrophilic activation. The presence of some σ^* character in the HOMO in Figure 11 right results in a weakened O–O bond which is activated for cleavage. Substrate coordination as in Figure 12b would contribute additional electron density

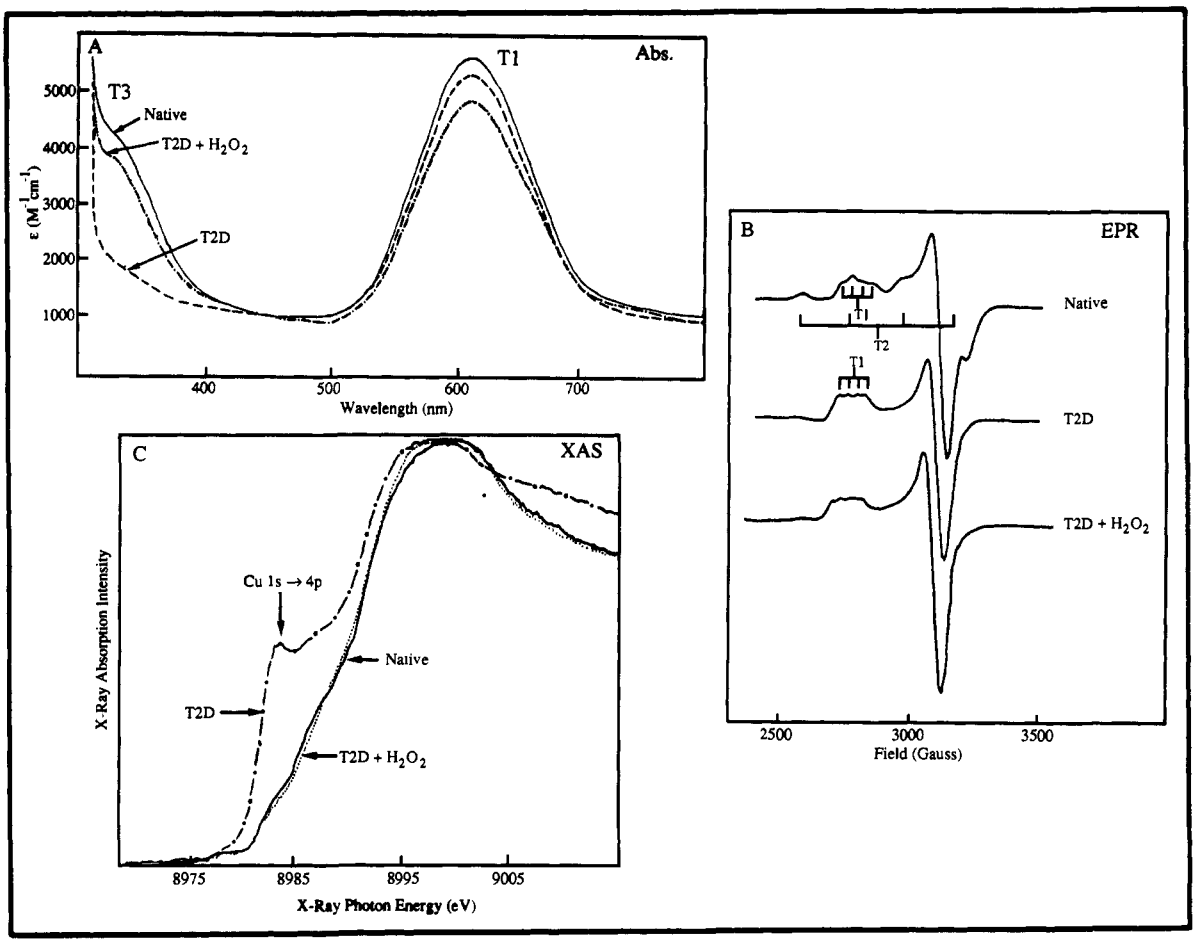

Figure 13. Spectroscopic comparison of native laccase, T2D laccase, and T2D reacted with excess H_2O_2: (A) absorption, (B) EPR, and (C) X-ray absorption spectra.

into the LUMO (Figure 11, right) which is antibonding with respect to both the O-O and Cu-O bonds and thus further facilitates the oxygen-transfer reaction. The important point here is that the side-on bridged structure results in a less negative peroxide but with a weaker O–O bond due to the fact that a small amount of electron density is accepted into a highly antibonding σ^* orbital on the peroxide.

V. Multicopper Oxidases

The multicopper oxidases (laccase[68] (one type 1 (T1), one type 2 (T2), one type 3 (T3)), ascorbate oxidase[69] (two T1, two T2, two T3), and ceruloplasmin[70] (two T1, one T2, one T3)) couple four one-electron oxidations of substrate at the T1 to the four-electron reduction of O_2 to water at the T2/T3, trinuclear copper cluster site.[4] The least complex of these oxidases is laccase which exhibits spectral contributions from each of the three types of copper (Figure 13). The T1 center is a fairly typical blue copper site exhibiting an intense cysteine $\pi \rightarrow$Cu(II) charge-transfer transition at 600 nm and an EPR signal with a small $A_\parallel$ value. This center and its involvement in long-range electron transfer to the trinuclear cluster has been discussed in section III. The T2 exhibits a normal EPR signal (i.e., large $A_\parallel$) which overlaps that of the T1 in Figure 13b, and the T3 is an antiferromagnetically coupled, EPR-inactive binuclear cupric center. The one spectral feature that has been associated with the T3 site is the 330-nm absorption band in Figure 13a. X-ray absorption edge and low-temperature MCD spectroscopies have proved to be valuable complements to absorption and EPR in defining the T2 and T3 sites in the multicopper oxidases and their reactions with O_2. These studies have shown that the T3 center is different from the coupled binuclear site in hemocyanin and tyrosinase, that the T2 and T3 together comprise a trinuclear copper cluster, and that this cluster is the minimum structural unit required for O_2 reactivity which generates two intermediates in the four-electron reduction of dioxygen to water. These studies are summarized below.

A. Coupled Binuclear/T3 Copper Site Comparison

Reversible removal of the T2 center from native laccase generates the type 2 depleted derivative (T2D)[71] which has allowed a chemical and spectroscopic comparison of the T3 center in laccase to the coupled site in hemocyanin.[72] From Figure 13a and b, T2D displays the spectral features assigned to the T1 but not the T2 centers. Importantly, the 330-nm band is not present in T2D but reappears on reaction with H_2O_2.[73] Two possible models could explain this behavior of the 330-nm band. Peroxide could be binding to an oxidized T3 site (i.e., in the met [Cu(II)Cu(II)] state) in T2D to produce an oxy-T3 site, with the 330-nm band being a $O_2^{2-} \rightarrow$Cu(II) charge-transfer transition.[74,75] This would parallel known hemocyanin chemistry where met + $H_2O_2 \rightarrow$ oxyhemocyanin. Alternatively, the T3 site in T2D could be reduced (i.e., in the deoxy[Cu(I)Cu(I)]

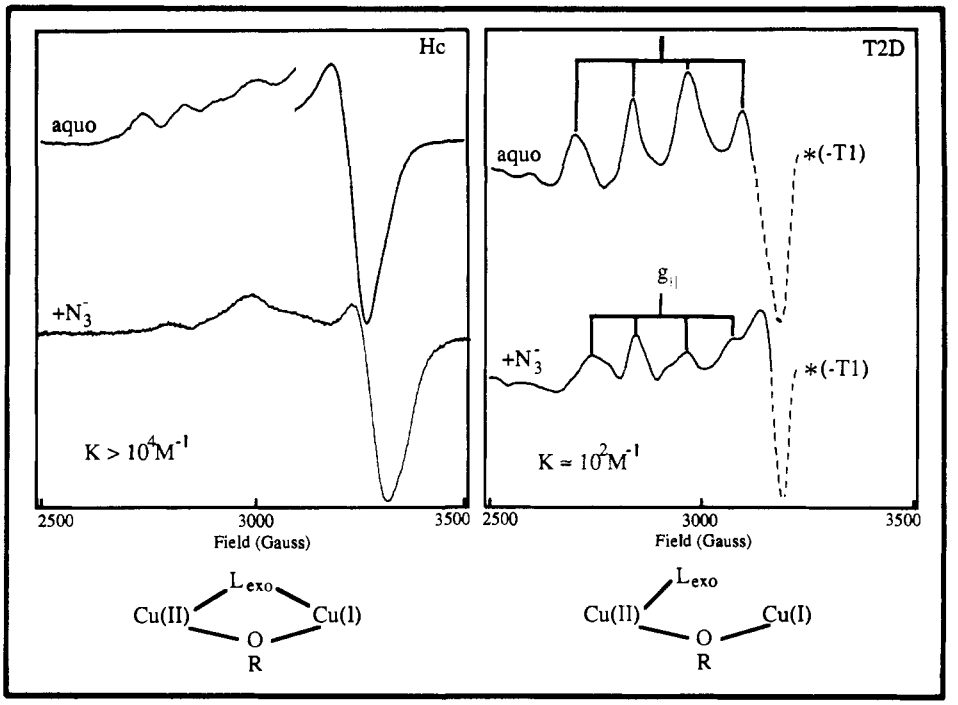

Figure 14. Exogenous ligand binding modes for Hc and T2D laccase. EPR spectra of (left) $^1/_2$-met hemocyanin (Hc) and (right) $^1/_2$-met T2D laccase without (top) and with (bottom) azide bound. The contribution from the type 1 copper of $^1/_2$-met T2D laccase has been eliminated by subtraction of the met T2D spectrum. The $g_\perp$ region is particularly sensitive to this subtraction; thus, the dashed part of the T2D spectrum should be viewed as approximate. Exogenous ligand binding models for each active site are given at the bottom.

state) even in the presence of O_2, but be oxidized by peroxide. XAS proved to be the ideal method to distinguish between these possibilities as it provides a direct spectroscopic probe of cuprous centers.[76] From Figure 13c, T2D exhibits a very low energy X-ray edge feature at 8984 eV, which we have shown to be characteristic of Cu(I), with a peak height which quantitates to a fully reduced T3 center. Reaction with H_2O_2 eliminates the 8984-eV peak, indicating that this deoxy T3 site has been oxidized to the met level. A peroxide titration showed that the disappearance of the 8984-eV peak linearly correlates with the appearance of the 330-nm absorption band requiring that the 330-nm band is associated with the met T3 site (an endogenous ligand-to-metal charge transfer transition) and that there is no evidence for peroxide binding to the met to form an oxy T3 derivative. Therefore, in contrast to hemocyanin the deoxy T3 site in laccase does *not* bind O_2 and the met T3 site does not bind peroxide. In parallel to hemocyanin the met T3 site in T2D laccase is strongly antiferromagnetically coupled, indicating the presence of an endogenous, likely OH^-, bridge which appears to be the ligand responsible for the 330 nm absorption band.[72]

The met hemocyanin and met T3 laccase sites can be reduced by one electron to generate the $^1/_2$met [Cu(II)Cu(I)] derivative which has provided key insight into differences in exogenous ligand binding between these proteins.[72] As shown in Figure 14, right, the $^1/_2$met T3 site exhibits normal Cu(II) EPR signals with four hyperfine components in the $g_\parallel$ region. Exogenous ligands such as azide bind to this site with equilibrium binding constants of $\sim 10^2$ M^{-1}, which are comparable to those of aqueous Cu(II). This is strikingly different from the data on $^1/_2$met hemocyanin which binds N_3^- with $K > 10^4$ M^{-1} producing a very unusual EPR spectrum (Figure 14, left). The unusual spectral features and high ligand binding affinities of the $^1/_2$met hemocyanin derivatives have been studied in detail in ref 77 and have been shown to result from the exogenous ligand bridging between the Cu(II) and Cu(I) of this mixed valence site. In contrast, the normal cupric chemical and spectral properties of the $^1/_2$met T3 derivative indicate that exogenous ligands binds only to the Cu(II) of this site. This difference in bridge vs terminal exogenous ligand binding (Figure 14, bottom) correlates with the differences in O_2 reactivity in that only deoxyhemocyanin reversibly binds dioxygen.

B. Trinuclear Copper Cluster Site

The T2 and T3 centers together are required for the O_2 reactivity of laccase[33] (vide infra). Low-temperature MCD (LTMCD) spectroscopy has provided important molecular level insight into the interactions of exogenous ligands with these centers relevant to the catalytic mechanism and first defined these centers to comprise a trinuclear copper cluster site.[4] The advantage of this physical method is that it allows an excited state spectral feature of a metal center to be correlated to its ground-state wave function. LTMCD intensity is governed by a C-term selection rule which requires a paramagnetic (i.e., $S > 0$) ground state.[78] Thus the T2 but not the antiferromagnetically coupled T3 center will exhibit intense LTMCD bands.

Titration of native laccase with azide produces two $N_3^- \rightarrow$Cu(II) charge-transfer bands in the absorption spectrum at 500 nm (weak) and 400 nm (intense) (Figure 15a, top).[4,79] The 400-nm band intensity is plotted as a function of N_3^- concentration in Figure 15b (dashed line). Correlation[4] to the LTMCD spectrum (Figure 15a, bottom) shows that there is an intense

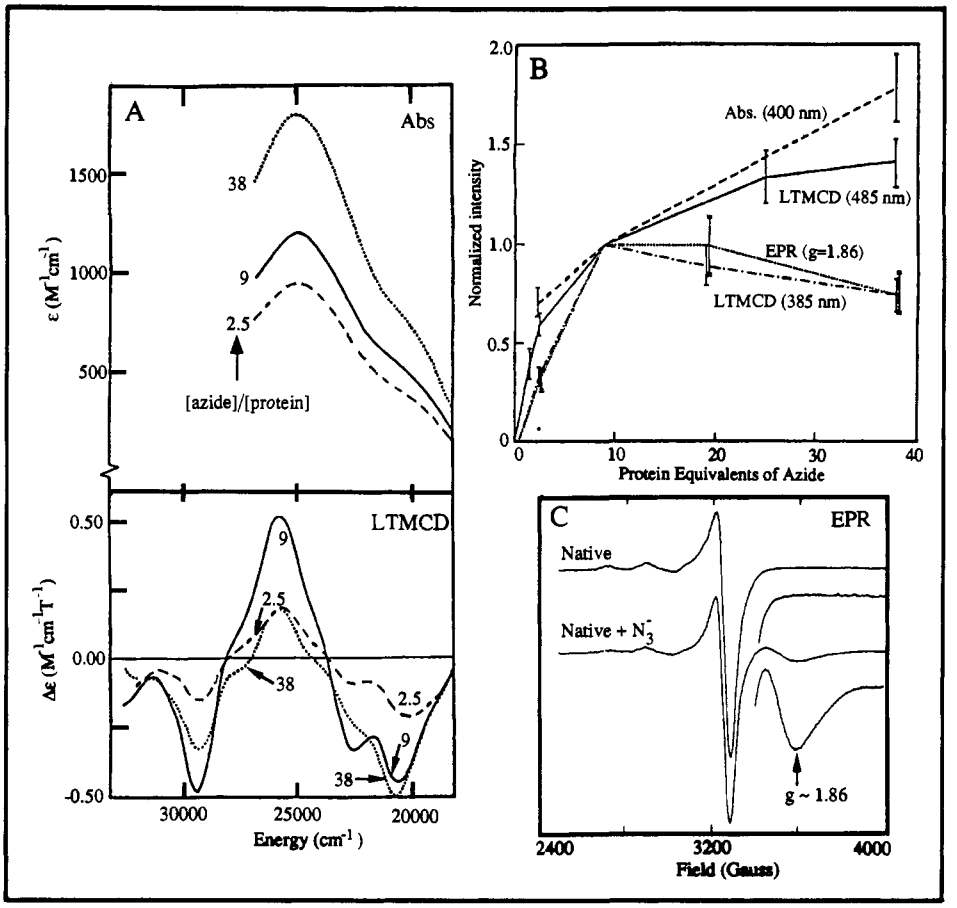

Figure 15. Spectroscopic effects of azide binding to the trinuclear copper site of native laccase: (A) absorption (top) and low-temperature MCD (bottom) and (C) EPR spectra. Panel B plots the effects of an azide titration on the magnitude of these spectroscopic features.

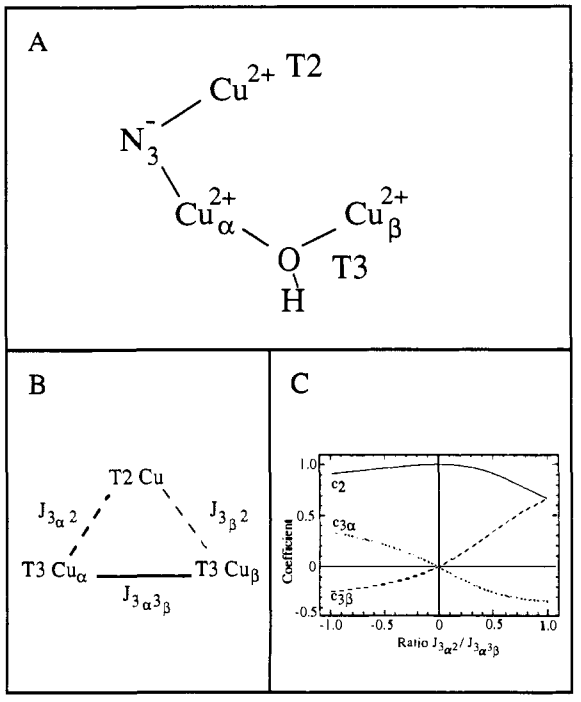

Figure 16. Geometric and electronic structure of the trinuclear copper site: (A) structural model for azide binding at the trinuclear cluster of laccase, (B) spin coupling model for the trinuclear cluster, and (C) dependence of EPR and MCD ground-state weighting coefficients on the exchange couplings in a Cu^{2+} trimer where $J_{3\beta 2} = 0$. Note that since $-J_{3_\alpha 3_\beta}$ is large and positive, positive ratios correspond to an antiferromagnetic $J_{3_\alpha 2}$, and negative ratios correspond to a ferromagnetic $J_{3_\alpha 2}$.

negative MCD feature at 485 nm which corresponds to the 500-nm absorption band and increases in magnitude with increasing N_3^- concentration (plotted in Figure 15b, solid line). Since it is intense in the LTMCD spectrum this band can be assigned as a charge transfer transition of azide bound to the T2 center. In the same energy region as the intense 400-nm absorption band, there is a positive LTMCD feature at ~385 nm. However, this MCD intensity first increases and then decreases with increasing azide concentration. This behavior is plotted in Figure 15b (dash-dot line) which shows that the 385-nm MCD band intensity does not correlate with the 400-nm absorption intensity. However, it does correlate with an unusual signal present in the EPR spectrum at $g = 1.86$ (Figure 15c; EPR intensity at $g = 1.86$ plotted in Figure 15b, dotted line). This $g = 1.86$ signal is associated with less than 10% of the T3 sites which are uncoupled due to protonation of the endogenous bridge at low pH in the presence of azide. The unusual g value derives from the fact that the uncoupled T3 site has two Cu(II) within 4 Å which dipole interact to produce a zero-field split triplet spectrum. The intense 400-nm absorption band thus has no corresponding LTMCD intensity and must be assigned as a charge-transfer transition of azide bound to a coupled T3 center.

From Figure 15b, azide binds to the T3 and T2 centers with similar binding constants, and a series of chemical perturbations have been performed which demonstrate that the 400- and 500-nm absorption bands

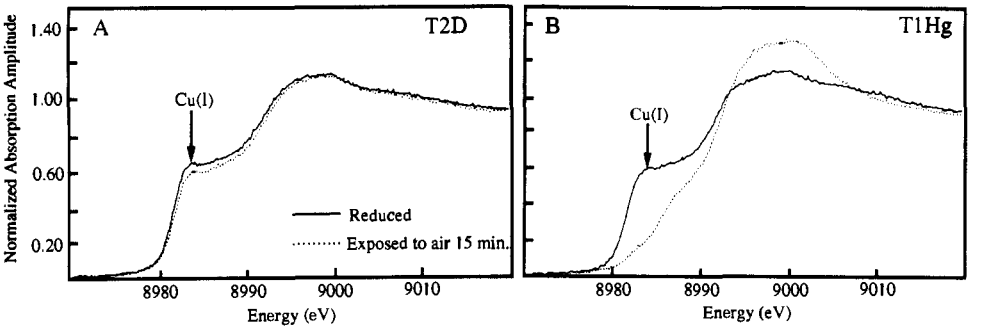

Figure 17. O_2 reactivity of laccase derivatives. X-ray absorption edges of fully reduced (solid) and air-exposed (dotted) T2D (A) and T1Hg (B) laccase derivatives.

are associated with the same azide. Thus one azide bridges between the T2 and T3 centers forming a trinuclear copper cluster as shown in Figure 16a. LTMCD spectroscopy first defined this new type of active site in biology,[4] which has recently been supported by X-ray crystallography on ascorbate oxidase.[34] It should be noted that LTMCD studies in the ligand-field region show[80] that the two coppers of the T3 center are somewhat inequivalent (Cu_α and Cu_β) with the bridging N_3^- binding to only the T3 Cu_α. The trinuclear copper cluster in ascorbate oxidase exhibits a similar T2/T3 N_3^- bridging geometry[81] supporting the involvement of this coordination mode in the O_2 reactivity of this center by providing an all inner-sphere electron-transfer pathway to the small molecule.

We complete this section by considering the electronic structure of this site, and in particular the fact that it is a trinuclear copper cluster, yet its spectral properties (EPR, MCD, etc.) have thus far been described as being T2 or T3 localized. The nature of the ground-state wave function of this cluster is dependent on superexchange bridging ligand pathways and has been analyzed[80] in terms of the spin-coupling model[82] in Figure 16b. The exchange Hamiltonian for the trimer is

$$H = -2J_{3_\alpha 3_\beta} S_{3_\alpha} \cdot S_{3_\beta} - 2J_{3_\alpha 2} S_{3_\alpha} \cdot S_2 - 2J_{3_\beta 2} S_{3_\beta} \cdot S_2$$

where $J_{3_\alpha 3_\beta}$ is the antiferromagnetic coupling between T3 Cu_α and T3 Cu_β, etc. and $J_{3_\alpha 3_\beta}$ is large ($-J > 400$ cm^{-1}, based on magnetic susceptibility studies on the met T3 site in T2D laccase) due to the hydroxide bridge in Figure 16a. If no ligand bridges between the T2 and T3 centers, $J_{3_\alpha 2} = J_{3_\beta 2} = 0$ and the $S = {}^1/_2$ ground-state wave function of the trimer clearly is localized on the T2 center with the T3 being an antiferromagnetically spin-coupled singlet that does not contribute, consistent with the spectral features of native laccase in Figure 13. It has been suggested from the crystal structure of ascorbate oxidase[34] that the native site might contain a μ_3-oxo or -hydroxo bridge which would correspond to $-J_{3_\alpha 2} = -J_{3_\beta 2} \neq 0$ but less than $-J_{3_\alpha 3_\beta}$ which still gives an $S = {}^1/_2$ ground-state localized on the T2 copper center. This T2/T3 interaction, if present, would affect the energies of the excited states of the trimer (three $S = {}^1/_2$'s couple to form $S_{total} = {}^1/_2$, ${}^1/_2$, and ${}^3/_2$ states), which however would be difficult to observe experimentally. While this would lead to a temperature dependence of the electronic structure, it would be complicated by the additional possibility of temperature-dependent geometric changes of the trinuclear copper cluster.[83]

The case of the asymmetric interaction of the T2 with one of the T3 coppers ($J_{3_\beta 2} = 0$; $-J_{3_\alpha 3_\beta} > -J_{3_\alpha 2} > 0$) is the most relevant since it relates to the azide-bridged structure in Figure 16a and one of the oxygen intermediates described in the next section. In this case the delocalization of the ground-state doublet is dependent on the relative magnitudes of $J_{3_\alpha 2}$ and $J_{3_\alpha 3_\beta}$ as shown in Figure 16c.[80] The coefficients in Figure 16c give the contributions of each copper in the cluster to the different spectral properties. For example, the g tensor of the ground-state doublet is given by $g_{trimer} = C_2 g_2 + C_{3_\alpha} g_{3_\alpha} + C_{3_\beta 3_\beta}$ where the g tensors of the individual ions (g_2 for T2, etc.) are expressed in the coordinate system of the trimer g tensor. For the azide-bridged site, the EPR, absorption and MCD features[80] are still consistent with the trimer doublet ground state being mostly localized on the T2, indicating that the coefficient of the T2 in Figure 16c is close to 1.0. Thus $J_{3_\alpha 2}/J_{3_\alpha 3_\beta} < 0.4$ which is consistent with the azide mediating an exchange coupling which is lower than that of the hydroxide bridge in Figure 16a. In contrast, the oxygen intermediate at the trinuclear copper site in native laccase (vide infra) has an $S = {}^1/_2$ ground state derived from the coupling of three $S = {}^1/_2$'s which exhibits spectral features considerably different from those of either a localized Cu(II) or an oxygen radical. These features would be consistent with a description of the ground state of this oxygen intermediate which is at the far right in Figure 16c with $J_{3_\alpha 2} \sim J_{3_\alpha 3_\beta}$.

C. Oxygen Reactivity and Intermediates

The copper ions and their oxidation states in laccase have been systematically varied in order to define the metal ions required for its O_2 reactivity. Earlier in this review, it was emphasized that XAS provides a powerful probe of the presence of Cu(I) on the basis of its peak at 8984 eV in the Cu K edge. This was used (Figure 13c) to show that deoxy T2D [$T1_{ox}T3_{red}$] does not react with dioxygen.[76] These studies were extended[33] to the fully reduced T2D derivative, [$T1_{red}T3_{red}$]. As shown by the lack of change in the 8984-eV peak in Figure 17a, this derivative does not react with dioxygen. This is an important result in that a [$T1_{red}T3_{red}$] site has been proposed to be the structural unit required for O_2 reduction[84] and mechanistic schemes in the literature have been based on this idea.[75,85] An additional laccase derivative has been prepared[86] and characterized[80,87] in which the T1 copper has been substituted with a spectroscopically and redox innocent mercuric ion. This T1Hg derivative contains a valid trinuclear copper cluster which, when fully reduced, [$T2_{red}T3_{red}$], rapidly

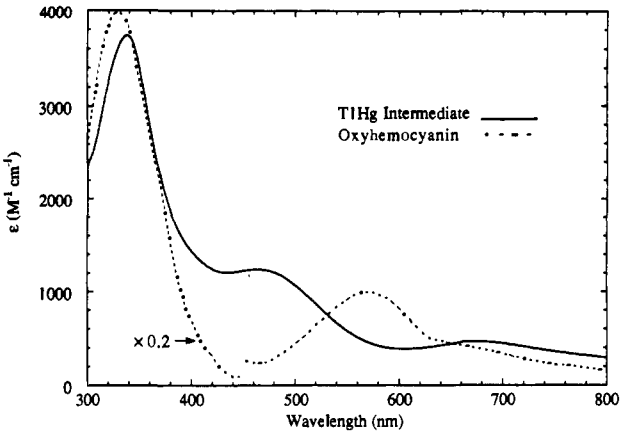

Figure 18. Absorption spectra of T1Hg laccase peroxide level intermediate (solid) and oxyhemocyanin (dashed). Note that the low-wavelength region of the oxyhemocyanin spectrum is scaled down 5-fold.

reacts with O_2 as shown by the disappearance of the 8984-eV peak in Figure 17b.[33] Thus the trinuclear copper cluster is, in fact, the minimum structural unit required for the multielectron reduction of dioxygen.

In the course of these studies we detected an intermediate in the reaction of reduced T1Hg laccase with dioxygen. A combination of CD/MCD/XAS spectroscopies have shown[88] that two electrons are initially transferred from the T3 coppers to dioxygen generating a peroxide level intermediate with $[T2_{red}T3_{ox}]$. The absorption spectrum of this intermediate (Figure 18) is strikingly different from that of oxyhemocyanin requiring a different mode of peroxide binding to the trinuclear copper cluster site. The $O_2^{2-} \rightarrow Cu(II)$ charge transfer intensity in laccase is ~5 fold weaker than in oxyhemocyanin and ~3 fold weaker than in the trans-μ-1,2 peroxide copper model complex,[46] indicating that the peroxide likely binds to only one of the T3 Cu(II), consistent with out results on the $^1/_2$met T2D derivative in Figure 14. The T1Hg peroxide intermediate spectrum is also not consistent with a terminal peroxide binding mode as the spectrum for such a complex (Figure 10b) shows no $O_2^{2-} \rightarrow Cu(II)$ charge transfer transition at energies above 500 nm. However, in Cu(II) hydroperoxide complexes $HO_2^- \rightarrow Cu(II)$ transitions are observed at higher energies (340–500 nm)[89] due to the strong bonding interaction of the proton with the π^* orbital. The fact that the reduced T3 site in deoxy T2D does not react with dioxygen indicates a major role for the T2 site in this reaction. We have proposed[88] that a μ-1,1 hydroperoxide bridges one of the oxidized T3 and the reduced T2 copper in the T1Hg laccase oxygen intermediate (Figure 19, structure A) which parallels the results for azide binding to the fully oxidized trinuclear copper cluster in Figure 16a. In contrast to hemocyanin (Figure 11, top) protonation of the bound peroxide in laccase is expected to lead to irreversible binding and promote further reduction to water. The unusually high affinity of exogenous ligands which bridge mixed-valent (Cu(II)–Cu(I)) binuclear sites[77] suggests that bridging to the reduced T2 copper stabilizes this oxygen intermediate. An attractive feature of this model is that μ-1,1 hydroperoxide binuclear cobalt complexes have been demonstrated to be most effective in further reduction to water.[90]

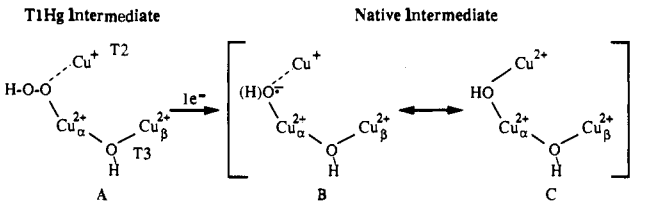

Figure 19. Proposed structural models of the T1Hg and native laccase oxygen intermediates.

An intermediate is also observed in the reaction of fully reduced native laccase $[T1_{red}T2_{red}T3_{red}]$ with O_2 in which the T1 as well as the T3 are oxidized based on the presence of their spectral features[91,92] as in Figure 13a and b. No T2 EPR signal is observed. The second-order rate constant for the formation of this intermediate is $1.7 \times 10^6\ M^{-1}\ s^{-1}$, while that for the formation of the peroxide intermediate in T1Hg laccase is $2.2 \times 10^6\ M^{-1}\ s^{-1}$.[88,91,92] Thus the peroxide intermediate appears to be a rate-limiting precursor to the native intermediate, the latter being at least one electron further reduced due to the additional oxidation of the T1 which occurs rapidly ($k > 1000\ s^{-1}$).[88] The native intermediate has been considered to be a three electron reduced oxygen radical (Figure 19, structure B). It exhibits an unusual EPR signal at liquid He temperature with a low g value of 1.9 which broadens when the intermediate is generated with $^{17}O_2$.[92,93] We have been able to prepare this intermediate in a form suitable for MCD spectroscopy using a rapid quench method and have found MCD to be a particularly powerful method for studying paramagnetic intermediates in a reaction mixture.[94] The low-temperature MCD spectrum of the native laccase intermediate is given in Figure 20, which shows three transitions at 318, 364, and 610 nm, the last being associated with the oxidized T1 copper. The 364-nm feature corresponds to a new band which is present in the absorption spectrum of the intermediate while the 318-nm band appears to correlate with the 330-nm absorption of the oxidized T3 site which has thus become paramagnetic in the intermediate. The temperature and field dependence of both bands (Figure 20, insert) show that these saturate with a $g = 1.94 \pm 0.05$ correlating both transitions with the $S = {}^1/_2$ ground state of the intermediate. The important point here is that a pure $S = {}^1/_2$ orbitally nondegenerate ground state such as would be present in the hydroxyl radical in Figure 19 (structure B) should have very little C term MCD intensity and its g value should not significantly deviate from 2.00. The high MCD intensity of the intermediate in Figure 20 requires significant Cu(II) character in the ground-state wave function, suggesting considerable electron delocalization onto the T2 copper as in Figure 19 (structure C) which is actually a four electron reduced oxygen product rather than a three electron reduced oxygen radical. Structure C, an hydroxide-bridged Cu(II) timer, would have similar antiferromagnetic coupling between both Cu(II) pairs ($J_{3_\alpha 2} \approx J_{3_\alpha 3_\beta}$ in Figure 16b,c) and a $S_{total} = {}^1/_2$ ground state delocalized over the three coppers. This structure would give MCD activity to the 330-nm T3 transition, and the EPR spectrum of this trimer would not resemble mononuclear Cu(II) or a radical. As discussed above, trimer g values contain contributions from the three cupric ions with the spin on the central copper opposing the other two spins (Figure 16c) which could

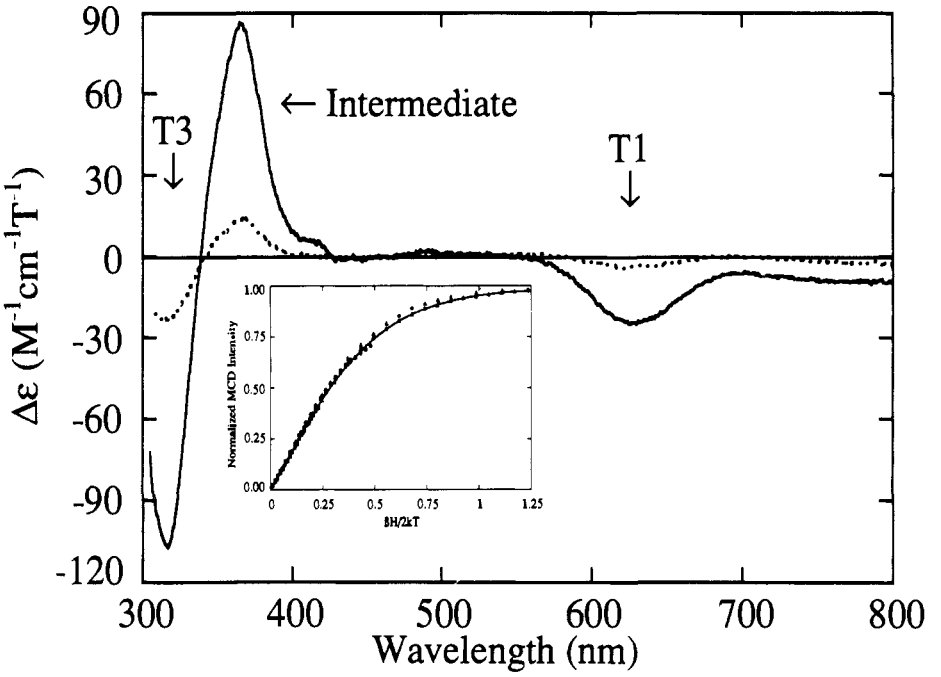

Figure 20. Low-temperature MCD spectra of the oxygen intermediate of native laccase. Spectra were taken at 4.2 (solid) and 25 K (dotted). Inset: MCD saturation magnetization data for the native laccase intermediate at a series of temperatures for the 318- and 364-nm features from 0–6 T. The solid line is a fit to all of the data for $S = {}^1/_2$ and $g_{eff} = 1.94$.

lead to a g value considerably below 2.00.

These results suggest that the four-electron reduction of dioxygen to water by laccase may proceed via two, two-electron steps to a product with different spectral properties from the resting enzyme. Subsequent loss of this T2/T3 hydroxide bridge would result in a T2 EPR signal and a diamagnetic T3 binuclear site as found in the resting enzyme. Experiments are underway to quantitate the nature of the ground-state wave function associated with this species (i.e., the relative contributions of structures B and C in Figure 19) to obtain a detailed description of its electronic structure.

VI. Future Directions

The unique spectral features of many of the copper proteins are now well understood. These have provided significant insight into the electronic and geometric structures of these active sites. These studies now allow one to focus on fundamental questions concerning electronic structure contributions to reactivity. For the blue copper sites, studies are being extended to the cuprous site to define changes in electronic structure upon reduction, to evaluate electronic contributions to the high reduction potentials of these sites and to obtain a more quantitative understanding of electronic contributions to electron transfer pathways, particularly between the T1 and the trinuclear copper cluster. For the coupled binuclear copper sites, studies now focus on detailed single-crystal spectroscopy on both the proteins and model complexes to correlate the electronic with the geometric structure and quantitatively understand electronic contributions to reversible O_2 binding and activation. With respect to the multicopper oxidases, a new trinuclear copper cluster site has now been defined as having a fundamentally different mode of peroxide binding to this site in the T1Hg intermediate relative to oxyhemocyanin, which must play a key role in the irreversible multielectron reduction of dioxygen to water. We are now extremely interested in defining in detail the electronic structures of this peroxide-level intermediate and the native intermediate and their contributions to catalysis.

VII. Abbreviations

CD	circular dichroism
ENDOR	electron nuclear double resonance
EPR	electron paramagnetic resonance
EXAFS	extended X-ray absorption fine structure
HOMO	highest occupied molecular orbital
LTMCD	low-temperature magnetic circular dichroism
LUMO	lowest unoccupied molecular orbital
SCF-Xα-SW	self-consistent field-Xα-scattered wave
T1Hg	mercury-substituted type 1 laccase derivative
T1	type 1 copper center
T2	type 2 copper center
T3	type 3 copper center
T2D	type 2 depleted laccase derivative
UV/vis	ultraviolet/visible
TDVC	transition dipole vector coupling
XAS	X-ray absorption spectroscopy

Acknowledgments. This research has been supported by the NSF (CHE-8919687 for the blue copper studies) and the NIH (DK-31450 for the coupled binuclear and multicopper protein studies). E.I.S. wishes to express his sincere appreciation to all his students and collaborators who are listed as co-authors in the literature cited for their commitment and major contributions to this science. It has been exciting!

VIII. References

(1) (a) Phenylalanine hydroxylase has a tetrahydropterin cofactor: Dix, T. A.; Benkovic, S. J. *Acc. Chem. Res.* **1988**, *21*, 101–107.

(b) Amine oxidase cofactor is 6-hydroxydopa (TOPA): Janes, S. M.; Wu, D.; Wemmer, D.; Smith, A. J.; Kaur, S.; Maltby, D.; Burlingame, A. L.; Klinman, J. P. *Science* **1990**, *248*, 981–987. (c) Galactose oxidase has an internal cofactor from a free radical at residue Tyr 272: Ito, N.; Phillips, S. E. V.; Stevens, C.; Ogel, Z. B.; McPherson, M. J.; Keen, J. N.; Yadav, K. D. S.; Knowles, P. F. *Nature* **1991**, *350*, 87–90.

(2) The Cu_A sites in cytochrome *c* oxidase and nitrous oxide reductase are similar, each with small hyperfine splitting, little imidazole nitrogen coupling, and an absorption band at 825 nm ($\epsilon \sim 2000\ M^{-1}\ cm^{-1}$) and 530 nm ($\epsilon \sim 6700\ M^{-1}\ cm^{-1}$), respectively. (a) For nitrous oxide reductase see: Jin, H.; Thomann, H.; Coyle, C. L.; Zumft, W. G. *J. Am. Chem. Soc.* **1989**, *111*, 4262–4269. Coyle, C. L.; Zumft, W. G.; Kroneck, P. M. H.; Körner, H.; Jakob, W. *Eur. J. Biochem.* **1985**, *153*, 459–467. (b) For cytochrome *c* oxidase see: Blair, D. F.; Martin, C. T.; Gelles, J.; Wang, H.; Brudvig, G. W.; Stevens, T. H.; Chan, S. I. *Chem. Scr.* **1983**, *21*, 43–53.

(3) (a) Solomon, E. I.; Penfield, K. W.; Wilcox, D. E. In *Structure and Bonding*; Hemmerich, P., et al., Eds.; Springer-Verlag: New York, 1983; pp 1–57. (b) Solomon, E. I. In *Copper Proteins*; Spiro, T. B., Ed.; Wiley: New York, 1981; pp 41–108. (c) Gray, H. B.; Solomon, E. I. In *Copper Proteins*; Spiro, T. B., Ed.; Wiley: New York, 1981; pp 1–39.

(4) (a) Allendorf, M. D.; Spira, D. J.; Solomon, E. I. *Proc. Natl. Acad. Sci. U.S.A.* **1985**, *82*, 3063–3067. (b) Spira-Solomon, D. J.; Allendorf, M. D.; Solomon, E. I. *J. Am. Chem. Soc.* **1986**, *108*, 5318–5328.

(5) Solomon, E. I. In *Comments on Inorganic Chemistry*; Sutin, N., Gütlich, P., Eds.; Gordon and Breach: New York, 1984; Vol. III, pp 227–320.

(6) Chow, C.; Chang, K.; Willett, R. D. *J. Chem. Phys.* **1973**, *59*, 2629–2640.

(7) (a) Johnson, K. H. *Adv. Quantum Chem.* **1973**, *7*, 143–183. (b) Slater, J. C. *The Calculation of Molecular Orbitals*; Wiley: New York, 1979. (c) Johnson, K. H.; Norman, J. G., Jr.; Connolly, J. W. D. In *Computational Methods for Large Molecules and Localized States in Solids*; Herman, F., McLean, A. D., Nesbet, R. K., Eds.; Plenum: New York, 1973; pp 161–201.

(8) Desjardins, S. R.; Penfield, K. W.; Cohen, S. L.; Musselman, R. L.; Solomon, E. I. *J. Am. Chem. Soc.* **1983**, *105*, 4590–4603.

(9) Gewirth, A. A.; Cohen, S. L.; Schugar, H. J.; Solomon, E. I. *Inorg. Chem.* **1987**, *26*, 1133–1146.

(10) Bencini, A.; Gatteschi, D. *J. Am. Chem. Soc.* **1983**, *105*, 5535–5541.

(11) Norman, J. G., Jr. *Mol. Phys.* **1976**, *31*, 1191–1198.

(12) (a) Herman, F.; Williams, A. R.; Johnson, K. H. *J. Chem. Phys.* **1974**, *61*, 3508–3522. (b) Yang, C. Y.; Johnson, K. H. *Int. J. Quant. Chem. S10* **1976**, 159–165. (c) Rösch, N.; Klemperer, W. G.; Johnson, K. H. *Chem. Phys. Lett.* **1973**, *23*, 149–154.

(13) Penfield, K. W.; Gewirth, A. A.; Solomon, E. I. *J. Am. Chem. Soc.* **1985**, *107*, 4519–4529.

(14) Didziulis, S. V.; Cohen, S. L.; Gewirth, A. A.; Solomon, E. I. *J. Am. Chem. Soc.* **1988**, *110*, 250–268.

(15) Hitchman, M. A.; Cassidy, P. J. *Inorg. Chem.* **1979**, *18*, 1745–1754.

(16) Solomon, E. I.; Gewirth, A. A.; Cohen, S. L. In *Understanding Molecular Properties*; Hansen, A. E., Avery, J., Dahl, J. P., Eds.; Reidel: Dordrecht, 1987; pp 27–68.

(17) In the SCF-Xα-SW method, the energy difference between the ground- and excited-state electronic configurations is computed by moving one-half a unit electronic charge from the ground-state spin orbital to an excited-state orbital and then reconverging the new potential to self-consistency. The energy difference between the spin orbitals is referred to at the transition-state energy and is to a very good approximation equal to the transition energy between the ground and excited states including electronic relaxation. Slater, J. C. *The Self-Consistent Field for Molecules and Solids: Quantum Theory of Molecules and Solids*; McGraw-Hill: New York, 1974; Vol. IV, pp 51–55.

(18) (a) Peisach, J.; Aisen, P.; Blumberg, W. E. In *The Biochemistry of Copper*; Academic Press: New York, 1966. (b) Vänngård, T. In *Biological Applications of Electron Spin Resonance*; Swartz, H. M., Bolton, J. R., Borg, D. C., Eds.; Wiley-Interscience: New York, 1972; pp 411–447. (c) Malmström, B. G., Reinhammer, B., Vänngård, T. *Biochem. Biophys. Acta* **1968**, *156*, 67–76.

(19) Solomon, E. I.; Hare, J. W.; Gray, H. B. *Proc. Natl. Acad. Sci. U.S.A.* **1976**, *73*, 1389–1393.

(20) Colman, P. M.; Freeman, H. C.; Guss, J. M.; Murata, M.; Norris, V. A.; Ramshaw, J. A. M.; Venkatappa, M. P. *Nature* **1978**, *272*, 319–324.

(21) (a) Adman, E. T.; Stenkamp, R. E.; Sieker, L. C.; Jensen, L. H. *J. Mol. Biol.* **1978**, *123*, 35–47. (b) Adman, E. T.; Turley, S.; Bramson, R.; Petratos, K.; Banner, D.; Tsernoglou, D.; Beppu, T.; Watanabe, H. *J. Biol. Chem.* **1989**, *264*, 87–99.

(22) (a) Norris, G. E.; Anderson, B. F.; Baker, E. N.; Rumball, S. V. *J. Mol. Biol.* **1979**, *135*, 309–312. (b) Norris, G. E.; Anderson, B. F.; Baker, E. N. *J. Mol. Biol.* **1983**, *165*, 501–521. (c) Norris, G. E.; Anderson, B. F.; Baker, E. N. *J. Am. Chem. Soc.* **1986**, *108*, 2784–2785. (d) Baker, E. N. *J. Mol. Biol.* **1988**, *203*, 1071–1095.

(23) Bergman, C.; Gandvik, E.-K.; Nyman, P. O.; Strid, L. *Biochem. Biophys. Res. Commun.* **1977**, *77*, 1052–1059.

(24) Thomann, H.; Bernardo, M.; Baldwin, M. J.; Lowery, M. D.; Solomon, E. I. *J. Am. Chem. Soc.* **1991**, *113*, 5911–5913.

(25) Penfield, K. W.; Gay, R. R.; Himmelwright, R. S.; Eickman, N. C.; Norris, V. A.; Freeman, H. C.; Solomon, E. I. *J. Am. Chem. Soc.* **1981**, *103*, 4382–4388.

(26) Gewirth, A. A.; Solomon, E. I. *J. Am. Chem. Soc.* **1988**, *110*, 3811–3819.

(27) Shadle, S. S.; Hedman, B.; Hodgson, K. O.; Solomon, E. I. To be published.

(28) (a) Scott, R. A.; Hahn, J. E.; Doniach, S.; Freeman, H. C.; Hodgson, K. O. *J. Am. Chem. Soc.* **1982**, *104*, 5364–5369. (b) Blair, D. F.; Campbell, G. W.; Schoonover, J. R.; Chan, S. I.; Gray, H. B.; Malmström, B. G.; Pecht, I.; Swanson, B. I.; Woodruff, W. H.; Cho, W. K.; English, A. M.; Fry, H. A.; Lum, V.; Norton, K. A. *J. Am. Chem. Soc.* **1985**, *107*, 5755–5766.

(29) Lowery, M. D.; Solomon, E. I. *Inorg. Chim. Acta*, in press.

(30) (a) Roberts, J. E.; Brown, T. G.; Hoffman, B. M.; Peisach, J. *J. Am. Chem. Soc.* **1980**, *102*, 825–829. (b) Brill, A. S.; Bryce, G. F. *J. Chem. Phys.* **1968**, *48*, 4398–4404. (c) Sharnoff, M. *J. Chem. Phys.* **1965**, *42*, 3383–3395.

(31) Bates, C. A.; Moore, W. S.; Standley, K. J.; Stevens, K. W. H. *Proc. Phys. Soc.* **1962**, *79*, 73–83.

(32) Kuki, A. In *Structure and Bonding*; Clarke, M. J., et al., Eds.; Springer-Verlag: Berlin, 1991; Vol. 75, pp 49–84.

(33) Cole, J. L.; Tan, G. O.; Yang, E. K.; Hodgson, K. O.; Solomon, E. I. *J. Am. Chem. Soc.* **1990**, *112*, 2243–2249.

(34) (a) Messerschmidt, A.; Rossi, A.; Ladenstein, R.; Huber, R.; Bolognesi, M.; Gatti, G.; Marchesini, A.; Petruzzelli, R.; Finazzi-Agrō, A. *J. Mol. Biol.* **1989**, *206*, 513–529. (b) Messerschmidt, A.; Huber, R. *Eur. J. Biochem.* **1990**, *187*, 341–352.

(35) Turley, S.; Adman, E. T.; Sieker, L. C.; Liu, M.-Y.; Payne, W. J.; LeGall, J. *J. Mol. Biol.* **1988**, *200*, 417–419.

(36) It should be noted that calculations on the reduced blue copper site show a similar orientation and aniostropic covalence in the ground state: Lowery, M. D.; Solomon, E. I. To be published.

(37) (a) Brown, J. M.; Powers, L.; Kincaid, B.; Larrabee, J. A.; Spiro, T. G. *J. Am. Chem. Soc.* **1980**, *102*, 4210–4216. (b) Co, M. S.; Hodgson, K. O.; Eccles, T. K.; Lontie, R. *J. Am. Chem. Soc.* **1981**, *103*, 984–986.

(38) (a) Solomon, E. I.; Dooley, D. M.; Wang, R.-H.; Gray, H. B.; Cerdonio, M.; Mogno, F.; Romani, G. L. *J. Am. Chem. Soc.* **1976**, *98*, 1029–1031. (b) Dooley, D. M.; Scott, R. A.; Ellinghaus, J.; Solomon, E. I.; Gray, H. B. *Proc. Natl. Acad. Sci. U.S.A.* **1978**, *75*, 3019–3022.

(39) Volbeda, A.; Hol, W. G. J. *J. Mol. Biol.* **1989**, *209*, 249–279.

(40) Eickman, N. C.; Himmelwright, R. S.; Solomon, E. I. *Proc. Natl. Acad. Sci. U.S.A.* **1979**, *76*, 2094–2098.

(41) Wilcox, D. E.; Clark, P. A.; Solomon, E. I. Unpublished results.

(42) Karlin, K. D.; Cruse, R. W.; Gultneh, Y.; Farooq, A.; Hayes, J. C.; Zubieta, J. *J. Am. Chem. Soc.* **1987**, *109*, 2668–2679.

(43) Pate, J. E.; Cruse, R. W.; Karlin, K. D.; Solomon, E. I. *J. Am. Chem. Soc.* **1987**, *109*, 2624–2630. In the present review, we use the term "monomer" to mean peroxide bound to a single copper center.

(44) Ross, P. K.; Allendorf, M. D.; Solomon, E. I. *J. Am. Chem. Soc.* **1989**, *111*, 4009–4021.

(45) Pate, J. E.; Ross, P. K.; Thamann, T. J.; Reed, C. A.; Karlin, K. D.; Sorrell, T. N.; Solomon, E. I. *J. Am. Chem. Soc.* **1989**, *111*, 5198–5209.

(46) Baldwin, M. J.; Ross, P. K.; Pate, J. E.; Tyeklár, Z.; Karlin, K. D.; Solomon, E. I. *J. Am. Chem. Soc.* **1991**, *113*, 8671–8679.

(47) Desjardins, S. R.; Wilcox, D. E.; Musselman, R. L.; Solomon, E. I. *Inorg. Chem.* **1987**, *26*, 288–300.

(48) Tuczek, F.; Solomon, E. I. To be published.

(49) (a) Karlin, K. D.; Cohen, B. I.; Hayes, J. C.; Farooq, A.; Zubieta, J. *Inorg. Chem.* **1987**, *26*, 147–153. (b) McKee, V.; Dagdigian, J. V.; Bau, R.; Reed, C. A. *J. Am. Chem. Soc.* **1981**, *103*, 7000–7001. (c) McKee, V.; Zvagulis, M.; Dagdigian, J. V.; Patch, M. G.; Reed, C. A. *J. Am. Chem. Soc.* **1984**, *106*, 4765–4772. (d) Sorrell, T. N.; O'Connor, C. J.; Anderson, O. P.; Reibenspies, J. H. *J. Am. Chem. Soc.* **1985**, *107*, 4199–4206.

(50) (a) Jacobson, R. R.; Tyeklár, Z.; Farooq, A.; Karlin, K. D.; Liu, S.; Zubieta, J. *J. Am. Chem. Soc.* **1988**, *110*, 3690–3692. (b) Ghosh, P.; Tyeklár, Z.; Karlin, K. D.; Jacobson, R. R.; Zubieta, J. *J. Am. Chem. Soc.* **1987**, *109*, 6889–6891.

(51) Kitajima, N.; Fujisawa, K.; Moro-oka, Y.; Toriumi, K. *J. Am. Chem. Soc.* **1989**, *111*, 8975–8976.

(52) Thompson, J. S. *J. Am. Chem. Soc.* **1984**, *106*, 4057–4059.

(53) Kitajima, N.; Koda, T.; Hashimoto, S.; Kitagawa, T.; Moro-oka, Y. *J. Chem. Soc., Chem. Commun.* **1988**, 151–152.

(54) Kitajima, N.; Fujisawa, K.; Fujimoto, C.; Moro-oka, Y.; Hashimoto, S.; Kitagawa, T.; Toriumi, K.; Tatsumi, K.; Nakamura, A. *J. Am. Chem. Soc.* **1992**, *114*, 1277–1291.

(55) Baldwin, M. J.; Pate, J. E.; Root, D. E.; Musselman, R. L.; Kitajima, N.; Solomon, E. I. To be published.
(56) (a) Magnus, K. A.; Lattman, E. E.; Volbeda, A.; Hol, W. G. J. *Proteins: Struct., Funct., Gene.* **1991**, *9*, 240–247. (b) The crystal structure of Limulus oxyhemocyanin subunit 2 has been further refined to 2.4-Å resolution: Magnus, K. A.; Ton-That, W. Personal communication.
(57) Polarized absorption and circular dichroism experiments on single crystals of oxyhemocyanin are currently in progress in our laboratory: Baldwin, M. J.; Mazzalupo, S. M.; Solomon, E. I. To be published.
(58) (a) Ross, P. K.; Solomon, E. I. *J. Am. Chem. Soc.* **1990**, *112*, 5871–5872. (b) Ross, P. K.; Solomon, E. I. *J. Am. Chem. Soc.* 1991, *113*, 3246–3259.
(59) (a) Noodleman, L.; Norman, J. G., Jr. *J. Chem. Phys.* **1979**, *70*, 4903–4906. (b) Noodleman, L. *J. Chem. Phys.* **1981**, *74*, 5737–5743.
(60) Hay, P. J.; Thibeault, J. C.; Hoffmann, R. *J. Am. Chem. Soc.* **1975**, *97*, 4884–4899.
(61) (a) Loehr, J. S.; Freedman, T. B.; Loehr, T. M. *Biochem. Biophys. Res. Commun.* **1974**, *56*, 510–515. (b) Freedman, T. B.; Loehr, J. S.; Loehr, T. M. *J. Am. Chem. Soc.* **1976**, *98*, 2809–2815. (c) Thamann, T. J.; Loehr, J. S.; Loehr, T. M. *J. Am. Chem. Soc.* **1977**, *99*, 4187–4189. (d) Larrabee, J. A.; Spiro, T. G.; Ferris, N. S.; Woodruff, W. H.; Maltese, W. A.; Kerr, M. S. *J. Am. Chem. Soc.* **1977**, *99*, 1979–1980. (e) Larrabee, J. A.; Spiro, T. G. *J. Am. Chem. Soc.* **1980**, *102*, 4217–4223.
(62) Jolley, R. L., Jr.; Evans, L. H.; Mason, H. S. *Biochem. Biophys. Res. Commun.* **1972**, *46*, 878–884.
(63) Jolley, R. L., Jr.; Evans, L. H.; Makino, N.; Mason, H. S. *J. Biol. Chem.* **1974**, *249*, 335–345.
(64) Himmelwright, R. S.; Eickman, N. C.; LuBien, C. D.; Lerch, K.; Solomon, E. I. *J. Am. Chem. Soc.* **1980**, *102*, 7339–7344.
(65) Winkler, M. E.; Lerch, K.; Solomon, E. I. *J. Am. Chem. Soc.* **1981**, *103*, 7001–7003.
(66) Wilcox, D. E.; Porras, A. G.; Hwang, Y. T.; Lerch, K.; Winkler, M. E.; Solomon, E. I. *J. Am. Chem. Soc.* **1985**, *107*, 4015–4027.
(67) (a) Karlin, K. D.; Hayes, J. C.; Gultneh, Y.; Cruse, R. W.; McKown, J. W.; Hutchinson, J. P.; Zubieta, J. *J. Am. Chem. Soc.* **1984**, *106*, 2121–2128. (b) Sorrell, T. N. *Tetrahedron* **1989**, *45*, 3–68.
(68) (a) Malmstrôm, B. G. In *New Trends in Bio-inorganic Chemistry*; Williams, R. J. P., Da Silva, J. R. R. F., Eds.; Academic Press: New York, 1978; Chapter 3. (b) Fee, J. A. *Struct. Bonding (Berlin)* **1975**, *23*, 1–60. (c) Reinhammar, B. In *Copper Proteins and Copper Enzymes*; Lontie, R., Ed.; CRC Press: Boca Raton, FL, 1984; Vol. III, Chapter 1. (d) Finazzi-Agrô, A. *Life Chem. Rep.* **1987**, *5*, 199–209. (e) Rydén, L. In *Copper Proteins and Copper Enzymes*; Lontie, R., Ed.; CRC Press: Boca Raton, FL, 1984; Vol. III, Chapter 2.
(69) Morpurgo, L.; Savini, I.; Gatti, G.; Bolognesi, M.; Avigliano, L. *Biochem. Biophys. Res. Commun.* **1988**, *152*, 623–628.
(70) (a) Musci, G.; Carbonaro, M.; Adriani, A.; Lania, A.; Galtieri, A.; Calabrese, L. *Arch. Biochem. Biophys.* **1990**, *279*, 8–13. (b) Calabrese, L.; Carbonaro, M.; Musci, G. *J. Biol. Chem.* **1989**, *264*, 6183–6187. (c) Calabrese, L.; Carbonaro, M.; Musci, G. *J. Biol. Chem.* 1988, *263*, 6480–6483.
(71) Graziani, M. T.; Morpurgo, L.; Rotilio, G.; Mondovì, B. *FEBS Lett.* **1976**, *70*, 87–90.
(72) Spira-Solomon, D. J.; Solomon, E. I. *J. Am. Chem. Soc.* **1987**, *109*, 6421–6432.
(73) LuBien, C. D.; Winkler, M. E.; Thamann, T. J.; Scott, R. A.; Co, M. S.; Hodgson, K. O.; Solomon, E. I. *J. Am. Chem. Soc.* **1981**, *103*, 7014–7016.
(74) (a) Farver, O.; Goldberg, M.; Lancet, D.; Pecht, I. *Biochem. Biophys. Res. Commun.* **1976**, *73*, 494–500. (b) Farver, O.; Goldberg, M.; Pecht, I. *FEBS Lett.* **1978**, *94*, 383–386.
(75) Farver, O.; Goldberg, M.; Pecht, I. *Eur. J. Biochem.* **1980**, *104*, 71–77.
(76) Kau, L.-S.; Spira-Solomon, D. J.; Penner-Hahn, J. E.; Hodgson, K. O.; Solomon, E. I. *J. Am. Chem. Soc.* **1987**, *109*, 6433–6442.
(77) Westmoreland, T. D.; Wilcox, D. E.; Baldwin, M. J.; Mims, W. B.; Solomon, E. I. *J. Am. Chem. Soc.* **1989**, *111*, 6106–6123.
(78) (a) Stephens, P. J. *Adv. Chem. Phys.* **1976**, *35*, 197–264. (b) Piepho, S. B.; Schatz, P. N. *Group Theory In Spectroscopy*; John Wiley and Sons, Inc.: New York, 1983.
(79) Morpurgo, L.; Rotilio, G.; Agrô, A. F.; Mondovì, B. *Biochim. Biophys. Acta* **1974**, *336*, 324–328.
(80) Cole, J. L.; Clark, P. A.; Solomon, E. I. *J. Am. Chem. Soc.* **1990**, *112*, 9534–9548. Note that the Cu_α and Cu_β notation for the type 3 site is opposite in the present review from that used in this reference in order to be consistent with more recent papers.
(81) Cole, J. L.; Avigliano, L.; Morpurgo, L.; Solomon, E. I. *J. Am. Chem. Soc.* **1991**, *113*, 8544–8546.
(82) (a) Banci, L.; Bencini, A.; Gatteschi, D. *Inorg. Chem.* **1983**, *22*, 2681–2683. (b) Banci, L.; Bencini, A.; Dei, A.; Gatteschi, D. *Inorg. Chem.* **1983**, *22*, 4018–4021. (c) Gatteschi, D.; Bencini, A. In *Magneto-Structural Correllations in Exchange Coupled Systems*; Willett, R. D., Gatteschi, D., Kahn, O., Eds.; NATO ASI Series, Reidel Publishing Co.: Dordrecht, The Netherlands, 1985; pp 241–268.
(83) (a) Li, J.-B.; McMillin, D. R.; Antholine, W. E. *J. Am. Chem. Soc.* **1992**, *114*, 725–727. (b) Morpurgo, L.; Agostinelli, E.; Senepa, M.; Desideri, A. *J. Inorg. Biochem.* **1985**, *24*, 1–8. (c) Severns, J. C.; McMillin, D. R. *Biochemistry* **1990**, *29*, 8592–8597.
(84) Reinhammer, B.; Oda, Y. *J. Inorg. Biochem.* **1979**, *11*, 115–127.
(85) (a) Reinhammer, B.; Malmström, B. G. In *Copper Proteins*; Spiro, T. G., Ed.; John Wiley & Sons: New York, 1981; Chapter 3. (b) Goldberg, M.; Farver, O.; Pecht, I. *J. Biol. Chem.* **1980**, 7353–7361.
(86) Morie-Bebel, M. M.; Morris, M. C.; Menzie, J. L.; McMillin, D. R. *J. Am. Chem. Soc.* **1984**, *106*, 3677–3678.
(87) (a) Morie-Bebel, M. M.; McMillin, D. R.; Antholine, W. E. *Biochem. J.* **1986**, *235*, 415–420. (b) Klemens, A. S.; McMillin, D. R.; Tsang, H.-T.; Penner-Hahn, J. E. *J. Am. Chem. Soc.* **1989**, *111*, 6398–6402.
(88) Cole, J. L.; Ballou, D. P.; Solomon, E. I. *J. Am. Chem. Soc.* **1991**, *113*, 8544–8546.
(89) Karlin, K. D.; Ghosh, P.; Cruse, R. W.; Farooq, A.; Gultneh, Y.; Jacobson, R. R.; Blackburn, N. J.; Strange, R. W.; Zubieta, J. *J. Am. Chem. Soc.* **1988**, *110*, 6769–6780.
(90) (a) Sykes, A. G.; Weil, J. A. *Prog. Inorg. Chem.* **1970**, *13*, 1–106. (b) Hoffman, A. B.; Taube, H. *Inorg. Chem.* **1968**, *7*, 1971–1976.
(91) Andréasson, L.-E.; Brändén, R.; Reinhammar, B. *Biochim. Biophys. Acta* **1976**, *438*, 370–379.
(92) Aasa, R.; Brändén, R.; Deinum, J.; Malmström, B. G.; Reinhammar, B.; Vänngård, T. *FEBS Lett.* **1976**, *61*, 115–119.
(93) Aasa, R.; Brändén, R.; Deinum, J.; Malmström, B. G.; Reinhammar, B.; Vänngård, T. *Biochem. Biophys. Res. Commun.* **1976**, *70*, 1204–1209.
(94) Clark, P. A.; Solomon, E. I. *J. Am. Chem. Soc.* **1992**, *114*, 1108–1110.